Research Square

Preprints are preliminary reports that have not undergone peer review.
They should not be considered conclusive, used to inform clinical practice,
or referenced by the media as validated information.

Female-predominant cardiac remodeling in type 2 diabetes mellitus and the estrogen–GPER–HIF-1α signaling pathway

Wanshi Liang
Zhujiang Hospital, Southern Medical University
Yongxian Ye
Zhujiang Hospital, Southern Medical University
Ying Zhong
Zhujiang Hospital, Southern Medical University
Yifei Chen
Zhujiang Hospital, Southern Medical University
Yali Song
Hengqin Hospital, First Affiliated Hospital of Guangzhou Medical University(Guangdong-Macao In-Depth Cooperation Zone in Hengqin central hospitals)
Zebin Yang
Zhujiang Hospital, Southern Medical University
Ronghao Luo
Foshan Hospital of Traditional Chinese Medicine (The Eighth Clinical Medical College of Guangzhou University of Chinese Medicine)
Yinhong Jie
Zhujiang Hospital, Southern Medical University
Hongyi Lei
Longgang Central Hospital
Yang Zhang
Southern Medical University, Nanfang Hospital
Le Li
lile2020@i.smu.edu.cn

Zhujiang Hospital, Southern Medical University

Research Article

Keywords: Sex differences, type 2 diabetes mellitus, left ventricular hypertrophy, diastolic function, GPER, estrogen, HIF-1α, db/db mice

Posted Date: October 27th, 2026

DOI: https://doi.org/10.21203/rs.3.rs-11363391/v1

License: This work is licensed under a Creative Commons Attribution 4.0 International License.
Read Full License

Additional Declarations:
No competing interests reported.

Tables 1 to 5 are available in the Supplementary Files section.

Female-predominant cardiac remodeling in type 2 diabetes mellitus and the estrogen–GPER–HIF-1α signaling pathway

Wanshi Liang[1,3]#, Yongxian Ye[1]#,Yin Zhong[1]#,Yifei Chen[1],Yali Song[4], Zebin Yang[1],Ronghao Luo[5], Yinhong Jie[1],Hongyi Lei[6],Yang Zhang[2]*, and Le Li[1]**

Background

Type 2 diabetes mellitus (T2DM) is associated with sex-specific cardiac remodeling, but the underlying clinical and molecular basis remains unclear. We investigated sex differences in left ventricular hypertrophy (LVH) and diastolic function and examined the role of estrogen–GPER and HIF-1α signaling in diabetic cardiac remodeling.

Methods

This retrospective cross-sectional study included 2,638 patients with T2DM (1,537 men and 1,101 women) evaluated between June 2023 and May 2024. LVH was defined using sex-specific left ventricular mass index thresholds, and sex differences were assessed using multivariable logistic regression. Cardiac remodeling was further evaluated in male and female db/db mice. Female db/db mice received 17β-estradiol (E2), the GPER antagonist G15, or the GPER agonist G1. High-glucose-treated H9c2 cardiomyoblasts were used for complementary pharmacological and HIF-1α reactivation experiments. Echocardiography, histology, molecular assays, transcriptomic profiling, and ubiquitination analysis were performed.

Results

LVH was more prevalent in women than in men with T2DM (27.8% vs. 9.5%, P<0.001), and women had a higher E/e′ ratio (median 10.99 vs. 9.86, P<0.001), whereas left ventricular ejection fraction was comparable. After adjustment for age, HbA1c, body mass index, and estimated glomerular filtration rate, female sex remained associated with LVH (odds ratio 3.71, 95% confidence interval 2.91–4.73, P<0.001). The sex-by-age-group interaction was not significant (P for interaction=0.405). Female db/db mice showed greater cardiac mass, wall thickening, fibrosis, cardiomyocyte hypertrophy, and diastolic impairment than male db/db mice. E2 and G1 attenuated these abnormalities, whereas G15 blunted the protective effects of E2. G1 reduced HIF-1α, ANGPT2, and VEGFA expression and increased HIF-1α ubiquitination. Pharmacological HIF-1α reactivation partially reversed the molecular and cellular effects of G1 in high-glucose-treated cardiomyoblasts.

Conclusions

Women with T2DM had a higher prevalence of LVH and greater diastolic dysfunction than men. The findings support a role for impaired estrogen–GPER signaling in female-predominant diabetic cardiac remodeling. GPER activation was associated with suppression of the HIF-1α/ANGPT2/VEGFA axis and may represent a potential therapeutic strategy.

Keywords: Sex differences; type 2 diabetes mellitus; left ventricular hypertrophy; diastolic function; GPER; estrogen; HIF-1α; db/db mice

Introduction

Diabetes mellitus (DM) is closely associated with structural and functional cardiac abnormalities. Left ventricular hypertrophy (LVH) is a common cardiac complication of DM and is associated with an increased risk of heart failure and myocardial infarction[1] Importantly, the cardiac consequences of DM may differ between women and men. In a large Italian population-based cohort, electrocardiography-defined LVH was more prevalent in women with type 2 diabetes mellitus (T2DM) than in men (23.5% vs. 8.4%), independent of age, body mass index, and blood pressure.[2] Similarly, data from the Framingham Study suggested that DM was associated with a greater relative excess risk of congestive heart failure in women than in men, with approximately fivefold and 2.4-fold increases, respectively.[3] These observations suggest that female sex may modify the cardiac remodeling response to T2DM; however, the biological mechanisms underlying this sex disparity remain incompletely understood.

The female-predominant cardiac burden in T2DM has traditionally been attributed, at least in part, to the loss of estrogen-mediated cardioprotection. Although premenopausal women generally have a lower risk of cardiovascular disease than men, this relative advantage appears to be attenuated in women with T2DM.[4] Nevertheless, available clinical and experimental evidence suggests that estrogen-related cardioprotection may not be completely abolished in the diabetic heart. Earlier menopause has been associated with an increased risk of heart failure, while menopause-related hormonal changes have been linked to concentric left ventricular remodeling and impaired diastolic function.[5-7] These findings support an association between declining estrogen exposure and adverse cardiac

remodeling, but they do not establish estrogen deficiency as the sole determinant of the female-predominant phenotype. In women with T2DM, age-related or menopause-associated reductions in estrogen may interact with chronic hyperglycemia, metabolic dysfunction, and other cardiovascular stressors, thereby contributing to the progressive development of LVH and diastolic impairment.

Experimental studies further indicate that estrogen receptor signaling remains functional under diabetic conditions. Pharmacological blockade of ERα and ERβ aggravates cardiovascular dysfunction in ovariectomized rats with T2DM.[8] Estrogen treatment has also been shown to preserve cardiac function and myocardial energy metabolism in a diabetes-related cardiomyopathy model.[9] In addition, ERβ has been reported to inhibit cardiac fibrosis.[10, 11] These findings suggest that estrogen signaling is not completely lost in the diabetic heart. However, the mechanisms underlying its insufficient cardioprotective effect remain unclear.

In addition to the classical nuclear estrogen receptors, estrogen also acts through G protein-coupled estrogen receptor 1 (GPER1, formerly known as GPR30), a seven-transmembrane receptor that mediates rapid, non-genomic signaling. GPER is expressed in cardiovascular tissues and is involved in the regulation of myocardial remodeling.[12] Activation of GPER has been shown to attenuate pressure overload-induced myocardial hypertrophy in ovariectomized mice.[13] However, whether GPER signaling is altered in the female diabetic heart and contributes to sex-related differences in cardiac remodeling remains unclear.

Hypoxia-inducible factor 1α (HIF-1α) is a key regulator of cellular responses to hypoxia and metabolic stress and has been implicated in cardiovascular disease, myocardial hypertrophy, and diabetic cardiomyopathy.[14]Previous evidence has shown that HIF-1α can upregulate GPER expression in cardiomyocytes,[15] suggesting a potential interaction between HIF-1α and estrogen-related signaling. Whether GPER regulates HIF-1α in the diabetic heart, and whether this interaction contributes to female-predominant cardiac remodeling, remains unknown.

In this study, we examined sex differences in LVH and diastolic function in patients with T2DM and compared cardiac remodeling between male and female db/db mice. We further investigated the effects of estrogen and GPER modulation in female db/db mice and high-glucose-treated H9c2 cells, with a particular focus on the potential involvement of HIF-1α-related signaling.

Method

Human Participants

This retrospective cross-sectional study included 2,638 patients with type 2 diabetes mellitus (T2DM), comprising 1,537 men and 1,101 women, who were evaluated between June 2023 and May 2024. T2DM was diagnosed according to the 1999 World Health Organization criteria [16].

Patients were excluded if they had: (1) Coronary artery disease，defined as >50% stenosis in a major epicardial coronary artery, a history of acute coronary syndrome, or previous

coronary revascularization; (2) uncontrolled hypertension, defined as systolic blood pressure ⩾140 mmHg and/or diastolic blood pressure ⩾90 mmHg despite antihypertensive treatment, a history of hypertensive emergency, or hypertension-related stroke; (3) moderate-to-severe valvular heart disease, congenital heart disease, or infectious, toxic, infiltrative, peripartum, or hypertrophic cardiomyopathy; (4) active autoimmune disease or a history of myocarditis; (5) severe pulmonary vascular disease; (6) a history of substance abuse; or (7) unavailable core clinical or echocardiographic records. This was a retrospective analysis of existing clinical data with no more than minimal risk to participants. The waiver of informed consent was approved by the Medical Ethics Committee of Zhujiang Hospital, Southern Medical University (2024-KY-285-02), in accordance with institutional policy and applicable regulatory criteria. The demographic and clinical details of enrolled participants are listed in Table 3.

In this study, left ventricular hypertrophy (LVH) was defined according to the left ventricular mass index (LVMI). Left ventricular mass was calculated from echocardiographic measurements of interventricular septal thickness, left ventricular end-diastolic diameter, and posterior wall thickness and was indexed to body surface area. LVH was defined as an LVMI >115 g/m² in men and >95 g/m² in women, according to the 2018 Chinese Guidelines for the Prevention and Treatment of Hypertension[17].

Animals and experimental design

Animal experiments were approved by the National Animal Care and Use Committee at Zhujiang Hospital of Southern Medical University, Guangzhou, China (Approval No.

LAEC-2024-010). All animal procedures adhered to the guidelines outlined in the National Research Council's Guide for the Care and Use of Laboratory Animals. Male and female db/db (BKS.Cg-Lepr$^{db/db}$/J) mice and their db/+ littermates (BKS.Cg-Lepr$^{db/+}$/J) mice as the control group were procured from Jakson's Lab. Mice were housed in under specific pathogen-free (SPF) conditions with controlled temperature (22 ± 2 °C), humidity (40-70%), and a 12/12 light-dark cycle. Body weight and blood glucose levels were monitored weekly via tail vein sampling using a glucometer (FreeStyle Optium Neo H, Abbott, UK). The protocols for genotyping db/db mice lines were conducted as previously described[18].

To investigate the effects and mechanisms of estrogen on cardiac fibrosis induced by T2DM, female db/db mice were randomly assigned to four experimental groups (n = 6): control (Ctrl) receiving subcutaneous DMSO; estrogen (E2) group receiving 30 μg/kg 17 β -estradiol; E2 + GPR30 inhibitor (E2 + G15) group receiving 30 μg/kg E2 and 0.5 mg/kg G15; and GPR30 agonist (G-1) group receiving 0.5 mg/kg G-1. Treatments were administered via subcutaneous injection three times weekly (Monday, Wednesday, Friday) for 10 weeks.

Cell culture and treatment

Rat cardiomyoblast H9c2 cells were obtained from the Cell Bank of the Chinese Academy of Sciences (Shanghai, China) and cultured in Dulbecco’s modified Eagle’s medium (DMEM) containing 10% fetal bovine serum and 1% penicillin/streptomycin at 37 °C in a 5% CO2 humidified incubator.

To establish a high-glucose stress model, H9c2 cells were cultured in medium containing 33 mM glucose for 48 h. Cells cultured in 5.5 mM glucose were used as the normal-glucose control.[19]

To evaluate the effects of estrogen and GPER signaling, high-glucose-treated cells were divided into four groups: the control group, which received the corresponding vehicle; the E2 group, which received 100 nM 17β-estradiol (E2); the E2+G15 group, which received 100 nM E2 and 10 μM G15; and the G1 group, which received 10 μM G1. G15 was used as a GPER antagonist, whereas G1 was used as a selective GPER agonist. All treatments were maintained for 48 h.

To further investigate the involvement of HIF-1α in GPER-mediated effects, high-glucose-treated cells were assigned to three groups: the HG group, the HG+G1 group, and the HG+G1+YC-1 group. G1 was used at 10 μM, and YC-1 was used at 10 μM. All treatments were maintained for 48 h. The role of YC-1 in modulating HIF-1α activity was interpreted according to the experimental design and the observed changes in HIF-1α expression.[20]

Echocardiography assessment for evaluation of cardiac function

Mice were anesthetized with isoflurane and maintained supine on a heating pad. Echocardiography was performed using a high-frequency linear array transducer. Structural and systolic parameters were measured by M-mode echocardiography in the parasternal long-axis view. These included left ventricular anterior wall thickness (LVAW), posterior wall thickness (LVPW), internal diameter at diastole (LVIDd) and systole (LVIDs).

Ejection fraction (EF) and fractional shortening (FS) were calculated from LVIDd and LVIDs. Left ventricular mass was derived using the Devereux formula.

Diastolic function was assessed by pulsed-wave Doppler in the apical four-chamber view. The sample volume was placed at the mitral valve tips. Peak early (E) and late (A) diastolic filling velocities were recorded, and the E/A ratio was calculated.

All measurements were averaged over three consecutive cardiac cycles by an investigator blinded to group allocation.

Heart weights

Both the heart weight index (heart weight/body weight ratio, HWI = HW/BW) and left ventricular weight index (left ventricular weight/body weight ratio, LVWI = LVW/BW) were calculated from the results of the associated measurements.

Histology and tissue staining

Morphological analysis of tissue sections was performed to more intuitively evaluate the level of hypertrophy and fibrosis in mouse myocardial tissues. The mouse heart was immediately placed in 10 % KCl to maintain diastole and subsequently transferred to a formalin solution for overnight fixation. After dehydration, the tissue was embedded in paraffin and cut into 5 μm slices. Tissue sections were stained with hematoxylin and eosin (H&E), wheat germ agglutinin (WGA) and Masson to assess the cross-sectional area of cardiomyocytes; picrosirius red and Masson trichrome staining were used to assess the level of myocardial fibrosis. Image analysis software (Image-Pro Plus, version 6.1.0) was used to analyze the digital images obtained after staining.

TUNEL Assay

The TUNEL mix was used to measure apoptotic rate. Myocardial sections were incubated with 50μL TUNEL mix at 37℃ for 1 h. DAPI staining was performed to visualize nuclei after the TUNEL reaction. The apoptosis ratio was expressed as the number of apoptotic myocytes (green) / total number of myocytes (blue) ×100%.

Quantitative Real-time polymerase chain reaction (qRT-PCR)

The mRNA expression levels of *Myh7,Col1a1, Nppa, Angpt2, Vegfa and Hif-α* in the heart were detected by qRT-PCR. Total RNA was extracted from myocardial tissues or H9c2 cells using the TRIzol Reagent and purified with Direct-zol RNA Kits (ZYMO, Irvine, CA, US). Reverse transcription was performed using the High-Capacity cDNA Reverse Transcription Kit (Thermo Fisher, Waltham, MA, USA). cDNA was amplified by Takara's Perfect Real-Time PCR Kit (Takara Bio, Otsu, Japan). Quantitative PCR was performed using the SYBR Green Premix Pro Taq HS qPCR Kit (Accurate Biotechnology) on a Bio-Rad CFX Connect system. Relative mRNA levels were normalized to Gapdh and expressed as a relative ratio. Primer sequences are provided in Table 2.

Western Blot Analysis

Proteins were extracted according to standard protocols and concentrations were determined using the BCA Protein Assay Kit (Beyotime, China). Equal amounts of protein (30-50 μg) were separated on 4-20% Tris-Glycine gels (Thermo Fisher, USA), and transferred to PVDF membranes (Millipore, USA). Membranes were incubated overnight at 4°C with primary antibodies:MYH7(1:1000,22280-1-AP,proteintech,China),

COL1A1(1:1000,HA722517,HUABIO,China), NPPA(1:500,A14755,ABconal,China), ANGPT2, VEGFa and HIF-1α(1:1000,NB100-105,Novus Biologicals,USA).

After TBST washing, membranes were incubated with HRP-conjugated secondary antibodies (1:10000) for 1.5 hours at room temperature. Protein bands were visualized using enhanced chemiluminescence reagents (Millipore, USA). GAPDH and Tubulin were used as loading controls.

RNA-seq

Total RNA was extracted from left ventricular tissues using TRIzol reagent. RNA samples were sequenced as described previously. The reads were mapped to the latest UCSC transcript set using Bowtie2 version 2.1.0[21] and the gene expression level was estimated using RSEM v1.2.15. TMM (trimmed mean of M-values) was Quality control testing was performed on all RNA samples using the Agilent 2100 Bioanalyzer, followed by polyadenylate positive (poly A+) selection and conversion to cDNA. After library construction, paired-end sequencing runs were performed on the Illumina HiSeq 2500. Genes with a fold change >2 (regardless of isoforms) and $P< 0.05$ were used for Gene Ontology analysis (http://david.abcc. ncifcrf. gov/).

Results

Sex differences in clinical characteristics and cardiac profiles

A total of 2,638 patients with T2DM were included in the clinical analysis, comprising 1,537 men and 1,101 women. Women were older than men (62.1 ± 10.9 vs. 58.7 ± 12.5 years, P<0.001) and had a longer duration of diabetes [6.0 (2.0–10.0) vs. 5.0 (1.0–10.0) years,

P=0.044]. HbA1c was lower in women than in men [7.2% (6.5–8.9%) vs. 7.6% (6.5–9.4%), P=0.003], whereas BMI did not differ significantly between the two groups (23.73 ± 3.79 vs. 23.95 ± 3.81 kg/m², P=0.154). The use of biguanides was more common among women, whereas the use of sulfonylureas and thiazolidinediones also differed between the sexes (Table 3).

LVH defined according to the sex-specific LVMI criteria was more prevalent in women than in men [305/1,097 (27.8%) vs. 146/1,532 (9.5%), P<0.001]. Using the exploratory LVPW-based criterion, LVH was also more common in women than in men [333/1,100 (30.3%) vs. 372/1,537 (24.2%), P<0.001]. Compared with men, women had smaller right and left ventricular dimensions, including lower RVD (1.99 ± 0.27 vs. 2.10 ± 0.28 cm, P<0.001) and LVD (4.04 ± 0.45 vs. 4.24 ± 0.49 cm, P<0.001). E/e′, used as the primary echocardiographic index of left ventricular filling pressure, was higher in women than in men [10.99 (9.14–13.26) vs. 9.86 (8.12–11.79), P<0.001], whereas LVEF was comparable between the two groups. Serum creatine kinase levels were lower in women, whereas LDH-L and HBDH levels were higher in women than in men (Table 3).

In the multivariable logistic regression model including sex, age, HbA1c, BMI, and eGFR, female sex remained independently associated with LVH (OR=3.71, 95% CI 2.91–4.73, P<0.001; n=2,196; 384 LVH events). BMI was positively associated with LVH (OR=1.06 per 1 kg/m² increase, 95% CI 1.03–1.09, P<0.001), whereas eGFR was inversely associated with LVH (OR=0.84 per 10 mL/min/1.73 m² increase, 95% CI 0.80–0.88, P<0.001). Age and HbA1c were not statistically significant in this model. The association between female sex

and LVH remained consistent after additional adjustment for diabetes duration (OR=3.42, 95% CI 2.55–4.60, P<0.001) and glucose-lowering medications (OR=3.67, 95% CI 2.67–5.04, P<0.001) (Table 3).

Age-stratified sex differences in cardiac abnormalities

Participants were further classified into three predefined age groups: <45 years, 45–55 years, and >55 years. These categories were used as age-defined strata and were not considered direct measures of menopausal status.

LVH defined by the LVMI criterion was more prevalent in women than in men across all three age groups: 10/65 (15.4%) vs. 6/188 (3.2%) in the <45-year group (P=0.001), 51/209 (24.4%) vs. 37/402 (9.2%) in the 45–55-year group (P<0.001), and 244/823 (29.6%) vs. 103/942 (10.9%) in the >55-year group (P<0.001) (Table 4). The corresponding crude odds ratios for LVH in women compared with men were 5.52 (95% CI 1.92–15.86), 3.18 (95% CI 2.00–5.06), and 3.43 (95% CI 2.66–4.42), respectively.

E/e′ was also higher in women than in men in the <45-year group [9.14 (8.00–10.62) vs. 8.49 (6.84–10.00), P=0.012], the 45–55-year group [10.60 (8.83–13.13) vs. 9.55 (7.88–11.45), P<0.001], and the >55-year group [11.25 (9.43–13.50) vs. 10.13 (8.50–12.29), P<0.001]. However, the sex-by-age-group interaction was not statistically significant in the multivariable model (P for interaction=0.405), indicating that the magnitude of the sex difference in LVH did not differ significantly across the predefined age strata.

Taken together, these findings show that women with T2DM had a higher prevalence of LVH and higher estimated left ventricular filling pressure than men. The association

between female sex and LVH remained significant after adjustment for available clinical covariates, although residual confounding cannot be excluded because blood pressure and antihypertensive-treatment data were not available in the dataset.

Female db/db Mice Exhibit cardiac remodeling at 22 Weeks

Because clinical analyses revealed a higher prevalence of left ventricular hypertrophy and more pronounced diastolic impairment in female patients with T2DM, we next investigated whether a similar phenotype could be reproduced in female diabetic mice. Longitudinal histological assessment from 4 to 22 weeks showed progressive myocardial remodeling in female db/db mice(Figure 1A). Based on these temporal findings, 22 weeks was selected for subsequent analyses. At this time point, gross examination showed an increase in heart size in db/db mice compared with controls (Figure 1B). Echocardiographic assessment further demonstrated thickened left ventricular walls in db/db mice, as reflected by increased left ventricular anterior wall thickness (LVAW) and left ventricular posterior wall thickness (LVPW), while left ventricular chamber dimension was relatively preserved (Figure 1C). Systolic function remained largely unchanged (Supplementary Figure 1), whereas diastolic function was impaired in db/db mice, as indicated by a reduced E/A ratio (Figure 1D). Histological analysis supported the presence of myocardial remodeling. Masson’s trichrome staining showed increased interstitial collagen deposition in db/db hearts (Figure 1E). Wheat germ agglutinin(WGA) staining revealed enlarged cardiomyocyte cross-sectional area, consistent with cardiomyocyte hypertrophy (Figure 1G). In line with these morphological

findings, protein expression of hypertrophic and fibrotic markers, including β-MHC, collagen I, and ANP, was increased in db/db myocardium (Figure 1F).

Collectively, these data indicate that female db/db mice exhibit a distinct cardiac remodeling phenotype at 22 weeks, characterized by left ventricular hypertrophy, diastolic dysfunction, and myocardial fibrosis.

Female db/db mice show more severe cardiac remodeling than males at 22 weeks

To determine whether sex influences the cardiac phenotype in db/db mice, female and male db/db mice were compared at 22 weeks. The HW/BW and LVW/BW was higher in female mice (Figure 2A), indicating greater overall cardiac mass. Echocardiographic analysis revealed increased LVPW thickness, and higher LV mass in females, while systolic function parameters were comparable between sexes (Supplementary Figure 2; Figure 2B). Assessment of diastolic function showed a lower E/A ratio in female mice, consistent with impaired diastolic relaxation and concordant with the clinical findings described above (Figure 2C).

Histological analyses demonstrated a more pronounced remodeling phenotype in female myocardium. Masson's trichrome staining showed a higher fibrotic area percentage in female mice (Figure 2D), and both HE and WGA staining revealed enlarged cardiomyocyte cross-sectional area compared with male db/db mice (Figure 2E).

At the molecular level, mRNA expression of the hypertrophic and fibrotic markers β-MHC, collagen I, and ANP was upregulated in female myocardium relative to males (Figure 2F).

These differences were corroborated at the protein level, with western blot analysis confirming higher expression of all three markers in female db/db hearts (Figure 2G). Taken together, these findings indicate that female db/db mice develop a more severe cardiac remodeling phenotype than males at 22 weeks, characterized by greater hypertrophy, interstitial fibrosis, and diastolic impairment.

Estrogen deficiency exacerbates cardiac remodeling in female db/db mice via GPER signaling

To investigate whether reduced estrogen contributes to the more severe cardiac phenotype observed in female db/db mice, we first assessed reproductive organ morphology and circulating estrogen levels. Female db/db mice exhibited marked uterine horn atrophy and ovarian atrophy compared with db/m controls (Figures 3A and 3B). Longitudinal measurement of serum estradiol (E2) levels revealed a progressive divergence between groups, with db/db mice showing significantly lower E2 levels at 22 weeks ($p = 0.0118$; Figure 3C), consistent with impaired ovarian estrogen production in the diabetic state.

To determine whether estrogen replacement could attenuate the cardiac phenotype, female db/db mice were treated with E2, the selective GPER agonist G1, or E2 combined with the GPER antagonist G15. E2 treatment reduced the heart weight-to-body weight ratio (HW/BW) compared with vehicle-treated controls, and this effect was abrogated by co-administration of G15 (Figure 3D). G1 alone similarly reduced HW/BW, suggesting that GPER activation is sufficient to mediate the cardioprotective effect of estrogen.

Histological assessment showed that myocardial fibrotic area was reduced in E2- and G1-treated mice relative to controls, whereas G15 co-treatment reversed the antifibrotic effect of E2 (Figure 3E). Echocardiographic evaluation of diastolic function demonstrated that the E/A ratio was significantly higher in E2- and G1-treated groups compared with controls, indicating improved diastolic relaxation, while E2+G15 co-treatment resulted in the lowest E/A ratio among all groups (all $p < 0.0001$; Figure 3F). Echocardiographic assessment of left ventricular wall thickness further supported these structural differences across treatment groups (Figure 3G).

At the molecular level, protein expression of β-MHC, collagen I, and ANP was reduced in E2- and G1-treated myocardium relative to controls, and was restored to elevated levels by G15 co-treatment (Figure 3H). Collectively, these findings indicate that the decline in estrogen observed in female db/db mice promotes cardiac remodeling, and that this process is at least in part mediated through GPER signaling.

High glucose induces hypertrophic and pro-apoptotic responses in H9c2 cardiomyocytes, which are attenuated by estrogen and GPER activation

To examine the cellular mechanisms underlying estrogen's cardioprotective effects, H9c2 cardiomyocytes were subjected to high glucose (HG) treatment as an in vitro model of diabetic cardiomyopathy. HG significantly upregulated the expression of hypertrophic and fibrotic markers β-MHC, collagen I, and ANP compared with normal glucose (NG) conditions (all $p < 0.0001$; Figure 4A), validating the in vitro model.

To assess the role of GPER signaling, HG-treated H9c2 cells were exposed to E2, the selective GPER agonist G1, or E2 combined with the GPER antagonist G15. E2 and G1 treatment both reduced BAX expression and increased BCL2 expression relative to vehicle-treated controls, indicating attenuation of apoptotic signaling. Co-administration of G15 reversed the effect of E2 on both BAX and BCL2, confirming that the anti-apoptotic action of estrogen is mediated through GPER (Figure 4B). Cell morphological changes and TUNEL staining further supported these findings (Figures 4C and 4D).

Consistently, E2 and G1 treatment markedly reduced the expression of β-MHC, collagen I, and ANP in HG-treated H9c2 cells, while G15 co-treatment restored these markers to elevated levels (all $p < 0.0001$; Figure 4E). These data indicate that estrogen suppresses high glucose-induced cardiomyocyte hypertrophy and apoptosis through GPER-dependent signaling.

GPER activation suppresses the HIF-1α/ANGPT2/VEGFA axis to protect against diabetic cardiomyopathy

As shown in Figure 4, G1-mediated GPER activation attenuated HG-induced hypertrophy and apoptosis in H9c2 cardiomyocytes. To identify the underlying molecular pathway, we performed transcriptomic profiling of cardiac tissue from db/db mice treated with G1 versus untreated controls. Heatmap and volcano plot analyses revealed distinct gene expression signatures between the two groups, with 59 upregulated and 73 downregulated genes identified in G1-treated hearts (Figures 5A and 5B). KEGG pathway enrichment analysis identified the HIF-1 signaling pathway as the most significantly suppressed pathway in

G1-treated cardiac tissue (Figure 5C), nominating HIF-1α and its downstream targets as candidate mediators of GPER-dependent cardioprotection in vivo.

To validate this transcriptomic finding, we directly examined HIF-1α and its canonical downstream effectors ANGPT2 and VEGFA in cardiac tissue. G1 treatment significantly reduced *Angpt2*, *Vegfa,* and *Hif-1α* mRNA levels compared with controls (all $P < 0.01$; Figure 6A), with concordant reductions confirmed at the protein level by western blot (ANGPT2: $P = 0.0007$; VEGFA: $P = 0.0058$; HIF-1α: $P = 0.0005$; Figure 6B). To determine the mechanism of HIF-1α downregulation, we performed co-immunoprecipitation with an anti-HIF-1α antibody followed by anti-ubiquitin immunoblotting. G1-treated hearts exhibited markedly enhanced ubiquitination of HIF-1α compared with controls (Figure 6C), indicating that GPER activation promotes proteasomal degradation of HIF-1α protein in vivo.

To directly establish a causal link between HIF-1α and GPER-mediated protection against diabetic cardiomyocyte injury, we performed a rescue experiment in HG-treated H9c2 cells using the HIF-1α stabilizer YC-1. Consistent with the in vivo findings, G1 significantly suppressed Angpt2, Vegfa, and Hif-1α mRNA and protein expression relative to HG controls (all $P < 0.0001$; Figures 7A and 7B). Co-treatment with YC-1 substantially reversed these G1-mediated reductions, restoring expression of all three targets toward HG levels. At the functional level, G1-induced attenuation of β-MHC, collagen I, and ANP expression was similarly reversed by YC-1 co-treatment (Figure 7C). Brightfield microscopy demonstrated that YC-1 reinstated cellular hypertrophy that had been suppressed by G1, and TUNEL staining confirmed that the G1-mediated reduction in apoptosis was abrogated upon HIF-1α

reactivation (Figures 7D and 7E). Collectively, these in vivo and in vitro data demonstrate that GPER activation protects against diabetic cardiomyopathy through ubiquitin-mediated degradation of HIF-1α and consequent suppression of the HIF-1α/ANGPT2/VEGFA signaling axis.

Discussion

In the present study, women with T2DM had a higher prevalence of LVH and a higher E/e′ ratio than men, while left ventricular systolic function was comparable between the sexes. Female sex remained associated with LVH after adjustment for age, HbA1c, BMI, and eGFR. A similar sex difference was observed in db/db mice, with female mice showing more pronounced cardiac hypertrophy, myocardial fibrosis, and diastolic impairment. In female db/db mice and high-glucose-treated H9c2 cardiomyoblasts, E2 treatment and GPER activation attenuated cardiac remodeling, whereas GPER antagonism weakened the protective effects of E2. Transcriptomic analysis suggested the involvement of HIF-1 signaling. G1 treatment reduced HIF-1α, ANGPT2, and VEGFA expression and increased HIF-1α ubiquitination. Moreover, YC-1 cotreatment partially reversed the molecular and cellular effects of G1 in high-glucose-treated cells. These findings suggest that estrogen–GPER signaling and the HIF-1α/ANGPT2/VEGFA pathway may be involved in the more severe cardiac remodeling observed in female diabetic models.

The clinical findings are consistent with previous epidemiological studies. The Casale Monferrato Study reported a higher prevalence of electrocardiography-defined LVH in women with T2DM than in men, independent of age, BMI, and blood pressure [2]. Similarly,

415 the Framingham Study showed that diabetes was associated with a greater relative
416 increase in the risk of heart failure in women than in men [3]. In our cohort, LVH defined
417 using sex-specific LVMI thresholds [22]was more common in women, and women had a
418 higher E/e′ ratio. E/e′ is an important echocardiographic variable for estimating left
419 ventricular filling pressure, although it should be interpreted together with other clinical and
420 echocardiographic findings[23, 24]. This pattern is broadly consistent with reports of less
421 favorable diastolic function in women with HFpEF and with reviews describing
422 estrogen-related mechanisms involved in diastolic reserve[25, 26]. The higher E/e′ ratio
423 therefore suggests a less favorable diastolic profile in women with T2DM rather than
424 establishing diastolic dysfunction by itself. LVH remained more prevalent in women in all
425 three age-defined strata, but the sex-by-age-group interaction was not significant. Because
426 menstrual status and circulating sex hormone levels were unavailable, these strata cannot
427 be regarded as premenopausal, perimenopausal, and postmenopausal groups. Thus, the
428 clinical data support a persistent sex difference in diabetic cardiac remodeling but do not
429 demonstrate that this difference increases during the menopausal transition.
430 The experimental findings were broadly consistent with the clinical observations. At 22
431 weeks, female db/db mice showed greater cardiac mass, wall thickening, myocardial fibrosis,
432 cardiomyocyte enlargement, and diastolic impairment than male db/db mice. Female db/db
433 mice also had reproductive organ atrophy and lower circulating E2 levels than db/m controls,
434 suggesting reduced estrogen availability in this model. E2 replacement and G1 treatment
435 improved the structural, functional, and molecular indices of remodeling, whereas G15

attenuated the effects of E2. These results are consistent with previous evidence that estrogen receptor signaling remains biologically active under diabetic conditions. [8, 9] However, because the present experiments used pharmacological agonism and antagonism without receptor-specific genetic manipulation, the data support a contribution of GPER but do not establish that GPER is the only estrogen receptor involved or that it is independently necessary and sufficient for cardioprotection.

The protective effects of GPER activation observed here are also in agreement with previous experimental studies. GPER activation attenuates myocardial hypertrophy and remodeling in pressure-overload models[12, 13]. In ovariectomized diabetic rats, Azizian et al. reported that G1 improved cardiac function and oxidative status through upregulation of the SIRT1/3–AMPK–UCP2 pathway.[27] Our results extend these observations to the db/db model and suggest an additional pathway involving HIF-1α and its downstream targets ANGPT2 and VEGFA. The beneficial response to E2 and G1 indicates that estrogen-related signaling is not completely lost in the diabetic heart. Instead, reduced estrogen availability and metabolic stress may limit endogenous protection, while pharmacological GPER activation can partly restore this response. Taken together, these studies suggest that GPER may regulate several complementary processes, including myocardial metabolism, oxidative stress, hypertrophic signaling, and fibrosis.

Transcriptomic analysis identified HIF-1 signaling as the most prominently enriched pathway among the genes altered by G1 treatment. The role of HIF-1α in the heart is context dependent: transient activation may support adaptation to ischemia, whereas sustained

457 dysregulation under chronic metabolic stress may contribute to adverse remodeling[14]. In
458 the present study, G1 reduced Hif-1α, Angpt2, and Vegfa at both the mRNA and protein
459 levels and increased HIF-1α ubiquitination. These findings suggest that GPER activation
460 may regulate HIF-1α through both transcriptional and post-translational mechanisms. The
461 increased ubiquitination supports enhanced targeting of HIF-1α for degradation, but direct
462 acceleration of proteasomal degradation cannot be inferred from co-immunoprecipitation
463 alone without protein half-life or proteasome-inhibition experiments. The inhibitory
464 association between estrogen–GPER signaling and cardiac HIF-1α is consistent with
465 findings in ovariectomized mice exposed to hypobaric hypoxia[28]. By contrast, GPER
466 stabilized HIF-1α through the PHD2/VHL pathway in tamoxifen-resistant breast cancer cells
467 [29], indicating that GPER–HIF-1α regulation is cell- and disease-context dependent. The
468 concomitant reduction in ANGPT2 and VEGFA is compatible with modulation of angiogenic
469 signaling, although microvascular function was not directly examined. Previous work
470 showed that HIF-1α can upregulate GPER in cardiomyocytes[15]; together with our findings,
471 this raises the possibility of reciprocal regulation, which requires direct testing. Finally,
472 although YC-1 co-treatment altered the molecular and cellular effects of G1, YC-1 is widely
473 used as an HIF-1 inhibitor rather than an HIF-1α stabilizer and also has HIF-independent
474 actions[30]. Therefore, these pharmacological findings should not be interpreted as
475 definitive HIF-1α reactivation or rescue until the compound identity and treatment design are
476 verified and the result is confirmed using genetic approaches.

Several limitations should be acknowledged. First, the clinical analysis was retrospective and cross-sectional and therefore cannot establish causality. Although the association between female sex and LVH remained significant in the available multivariable and sensitivity models, blood pressure, antihypertensive treatment, menopausal status, and circulating sex hormone levels were unavailable, leaving potential residual confounding. Second, the age categories were surrogate strata rather than confirmed reproductive stages, and no longitudinal cardiovascular outcomes were assessed. Third, the db/db model combines obesity, hyperglycemia, leptin-receptor deficiency, and reduced estrogen levels; ovariectomized models and tissue-specific GPER knockout models are needed to separate these effects. Fourth, H9c2 cells are embryonic rat cardiomyoblasts and do not fully reproduce adult human cardiomyocyte biology. Validation in primary adult or induced pluripotent stem cell-derived cardiomyocytes is required. Fifth, the E3 ligase responsible for HIF-1α ubiquitination was not identified, and the pharmacological specificity and direction of the YC-1 experiment require further confirmation. Genetic rescue with HIF-1α overexpression or a degradation-resistant HIF-1α mutant, together with proteasome-inhibition and protein half-life assays, would strengthen the proposed mechanism.

In conclusion, women with T2DM had a higher prevalence of LVH and a less favorable diastolic profile than men, and female db/db mice developed more severe cardiac remodeling than male mice. The experimental findings indicate that estrogen–GPER signaling may attenuate diabetic cardiac hypertrophy, fibrosis, and apoptosis and identify

the HIF-1α/ANGPT2/VEGFA axis as a potential downstream pathway. Further genetic and pharmacological validation is needed before GPER or HIF-1α-related signaling can be considered a sex-specific therapeutic target in T2DM.

Acknowledgements

The authors thank all patients for their permission to use their clinical data in this study

Author contributions

WSL and YZ conducted the experiments and performed data analysis; YXY collected patient samples analyzed the clinical data;YFC and YLS provided experimental and technical support;ZBY and RHL revised the manuscript;YHJ perfromed data interpretation and visualization; HYL provided financial support; YZ and LL designed the experiments, acquired funding, and edited the manuscript. All authors read and approved the final manuscript.

Funding

This research was supported by grants from the National Natural Science Foundation of China [No.82171357], the Natural Science Foundation of Guangdong Province [No.2025A1515012073] and Shenzhen Science and Technology Program [No. JCYJ20240813114628037].

Declarations

Ethics approval and consent to participate

All procedures in this study were reviewed and approved by the Laboratory Animal Ethics Committee (Approval No. LAEC-2024-010) and Medical Ethics Committee (Approval No. 2024-KY-285-02) of Zhujiang Hospital, Southern Medical University, Guangzhou, China

Consent for publication

Not applicable.

Competing interests

The authors declare no competing interests.

Author details

1.Department of Anesthesiology, Zhujiang Hospital, Southern Medical University, Guangzhou, Guangdong, 510282, China
2.Division of Orthopaedic Surgery, Department of Orthopaedics, Southern Medical University, Nanfang Hospital, Guangzhou, Guangdong, 510515, China
3.Department of Anesthesiology,Sun Yat-sen Memorial Hospital, Sun Yat-sen University,Guangzhou, Guangdong, 510180, China
4.Department of Anesthesiology, Hengqin Hospital, First Affiliated Hospital of Guangzhou Medical University(Guangdong-Macao In-Depth Cooperation Zone in Hengqin central hospitals), Zhuhai, Guangdong, 519031, China
5.Department of Anesthesiology, Foshan Hospital of Traditional Chinese Medicine (The Eighth Clinical Medical College of Guangzhou University of Chinese Medicine), Foshan, 528000,China
#These authors contributed equally to this work.
6.Department of Anesthesiology, Longgang Central Hospital of Shenzhen, Shenzhen, Guangdong, 510006, China

**Le Li is the paper's lead contact.

Corresponding Author: Le Li; Tel: +86-13242805989; E-mail: lile2020@i.smu.edu.cn; Address: No. 253 Gongye Da Rd., Guangzhou, Guangdong, 510282, China

Co-corresponding Author: Yang Zhang; Tel: +86-13242805989; E-mail: zhangyangdemail@foxmail.com; Address: No. 1838 Guangzhou Da Rd., Guangzhou, Guangdong, 510515, China

1. Jia G, Hill MA, Sowers JR. Diabetic Cardiomyopathy: An Update of Mechanisms Contributing to This Clinical Entity. Circ Res. 2018;122(4):624-38.https://doi.org/10.1161/circresaha.117.311586

2. Bruno G, Giunti S, Bargero G, Ferrero S, Pagano G, Perin PC. Sex-differences in prevalence of electrocardiographic left ventricular hypertrophy in Type 2 diabetes: the Casale Monferrato Study. Diabet Med. 2004;21(8):823-8.https://doi.org/10.1111/j.1464-5491.2004.01246.x

3. Kannel WB, Hjortland M, Castelli WP. Role of diabetes in congestive heart failure: the Framingham study. Am J Cardiol. 1974;34(1):29-34.https://doi.org/10.1016/0002-9149(74)90089-7

4. Fourny N, Beauloye C, Bernard M, Horman S, Desrois M, Bertrand L. Sex Differences of the Diabetic Heart. Front Physiol. 2021;12:661297.https://doi.org/10.3389/fphys.2021.661297

5. Muka T, Asllanaj E, Avazverdi N, Jaspers L, Stringa N, Milic J, et al. Age at natural menopause and risk of type 2 diabetes: a prospective cohort study. Diabetologia. 2017;60(10):1951-60.https://doi.org/10.1007/s00125-017-4346-8

6. Sung KT, Chandramouli C, Lo CI, Tsai JP, Lai YH, Hsiao CC, et al. Association of Female Menopause With Atrioventricular Mechanics and Outcomes. Front Cardiovasc Med. 2022;9:804336.https://doi.org/10.3389/fcvm.2022.804336

7. Maslov PZ, Kim JK, Argulian E, Ahmadi A, Narula N, Singh M, et al. Is Cardiac Diastolic Dysfunction a Part of Post-Menopausal Syndrome? JACC Heart Fail. 2019;7(3):192-203.https://doi.org/10.1016/j.jchf.2018.12.018

8. Azizian H, Farhadi Z, Khaksari M. Selective estrogen receptor α and β antagonist aggravate cardiovascular dysfunction in type 2 diabetic ovariectomized female rats. Horm Mol Biol Clin Investig. 2022;43(4):427-36.https://doi.org/10.1515/hmbci-2021-0073

9. Yan H, Yang W, Zhou F, Pan Q, Allred K, Allred C, et al. Estrogen Protects Cardiac Function and Energy Metabolism in Dilated Cardiomyopathy Induced by Loss of Cardiac IRS1 and IRS2. Circ Heart Fail. 2022;15(6):e008758.https://doi.org/10.1161/circheartfailure.121.008758

10. Pedram A, Razandi M, Narayanan R, Levin ER. Estrogen receptor beta signals to inhibition of cardiac fibrosis. Mol Cell Endocrinol. 2016;434:57-68.https://doi.org/10.1016/j.mce.2016.06.018

11. Pedram A, Razandi M, O'Mahony F, Lubahn D, Levin ER. Estrogen receptor-beta prevents cardiac fibrosis. Mol Endocrinol. 2010;24(11):2152-65.https://doi.org/10.1210/me.2010-0154

12. Wang Z, Liu J, Chen Y, Tang Y, Chen T, Zhou C, et al. From physiology to pathology: Emerging roles of

GPER in cardiovascular disease. Pharmacol Ther. 2025;267:108801.https://doi.org/10.1016/j.pharmthera.2025.108801
13. Zhang S, Ma J, Wang X, Zhao D, Zhang J, Jiang L, et al. GPR30 Alleviates Pressure Overload-Induced Myocardial Hypertrophy in Ovariectomized Mice by Regulating Autophagy. Int J Mol Sci. 2023;24(2).https://doi.org/10.3390/ijms24020904
14. Sato T, Takeda N. The roles of HIF-1α signaling in cardiovascular diseases. J Cardiol. 2023;81(2):202-8.https://doi.org/10.1016/j.jjcc.2022.09.002
15. Recchia AG, De Francesco EM, Vivacqua A, Sisci D, Panno ML, Andò S, et al. The G protein-coupled receptor 30 is up-regulated by hypoxia-inducible factor-1alpha (HIF-1alpha) in breast cancer cells and cardiomyocytes. J Biol Chem. 2011;286(12):10773-82.https://doi.org/10.1074/jbc.M110.172247
16. Alberti KG, Zimmet PZ. Definition, diagnosis and classification of diabetes mellitus and its complications. Part 1: diagnosis and classification of diabetes mellitus provisional report of a WHO consultation. Diabet Med. 1998;15(7):539-53.https://doi.org/10.1002/(sici)1096-9136(199807)15:7<539::Aid-dia668>3.0.Co;2-s
17. 2018 Chinese Guidelines for Prevention and Treatment of Hypertension-A report of the Revision Committee of Chinese Guidelines for Prevention and Treatment of Hypertension. J Geriatr Cardiol. 2019;16(3):182-241.https://doi.org/10.11909/j.issn.1671-5411.2019.03.014
18. Friedman JM, Halaas JL. Leptin and the regulation of body weight in mammals. Nature. 1998;395(6704):763-70.https://doi.org/10.1038/27376
19. Sun HJ, Xiong SP, Wu ZY, Cao L, Zhu MY, Moore PK, et al. Induction of caveolin-3/eNOS complex by nitroxyl (HNO) ameliorates diabetic cardiomyopathy. Redox Biol. 2020;32:101493.https://doi.org/10.1016/j.redox.2020.101493
20. Zhang Y, Liu D, Hu H, Zhang P, Xie R, Cui W. HIF-1α/BNIP3 signaling pathway-induced-autophagy plays protective role during myocardial ischemia-reperfusion injury. Biomed Pharmacother. 2019;120:109464.https://doi.org/10.1016/j.biopha.2019.109464
21. Langmead B, Salzberg SL. Fast gapped-read alignment with Bowtie 2. Nat Methods. 2012;9(4):357-9.https://doi.org/10.1038/nmeth.1923
22. Lang RM, Badano LP, Mor-Avi V, Afilalo J, Armstrong A, Ernande L, et al. Recommendations for cardiac chamber quantification by echocardiography in adults: an update from the American Society of Echocardiography and the European Association of Cardiovascular Imaging. Eur Heart J Cardiovasc Imaging. 2015;16(3):233-70.https://doi.org/10.1093/ehjci/jev014
23. Nagueh SF, Smiseth OA, Appleton CP, Byrd BF, 3rd, Dokainish H, Edvardsen T, et al. Recommendations for the Evaluation of Left Ventricular Diastolic Function by Echocardiography: An Update from the American Society of Echocardiography and the European Association of Cardiovascular Imaging. J Am Soc Echocardiogr. 2016;29(4):277-314.https://doi.org/10.1016/j.echo.2016.01.011
24. Nagueh SF, Sanborn DY, Oh JK, Anderson B, Billick K, Derumeaux G, et al. Recommendations for the Evaluation of Left Ventricular Diastolic Function by Echocardiography and for Heart Failure With Preserved Ejection Fraction Diagnosis: An Update From the American Society of Echocardiography. J Am Soc Echocardiogr. 2025;38(7):537-69.https://doi.org/10.1016/j.echo.2025.03.011
25. Sotomi Y, Hikoso S, Nakatani D, Mizuno H, Okada K, Dohi T, et al. Sex Differences in Heart Failure With Preserved Ejection Fraction. J Am Heart Assoc. 2021;10(5):e018574.https://doi.org/10.1161/jaha.120.018574
26. Du J, Liu J, Wang X, Wang X, Ma Y, Zhang S, et al. The role of estrogen in the sex difference for the risk factors of heart failure with preserved ejection fraction. Biol Direct.

2025;20(1):28.https://doi.org/10.1186/s13062-025-00618-x
27. Azizian H, Farhadi Z, Bader M, Alizadeh Ghalenoei J, Ghafari MA, Mahmoodzadeh S. GPER activation attenuates cardiac dysfunction by upregulating the SIRT1/3-AMPK-UCP2 pathway in postmenopausal diabetic rats. PLoS One. 2023;18(12):e0293630.https://doi.org/10.1371/journal.pone.0293630
28. Wowui PI, Mprah R, Ndzie Noah ML, Adu-Amankwaah J, Kanoseh AWL, Tao L, et al. Estrogen via GPER downregulated HIF-1a and MIF expression, attenuated cardiac arrhythmias, and myocardial inflammation during hypobaric hypoxia. Mol Med. 2025;31(1):107.https://doi.org/10.1186/s10020-025-01144-2
29. Zhang Y, Song Y, Ren S, Zhang M, Zhang Z, Fan S, et al. GPER-mediated stabilization of HIF-1α contributes to upregulated aerobic glycolysis in tamoxifen-resistant cells. Oncogene. 2023;42(3):184-97.https://doi.org/10.1038/s41388-022-02506-4
30. Yeo EJ, Chun YS, Cho YS, Kim J, Lee JC, Kim MS, et al. YC-1: a potential anticancer drug targeting hypoxia-inducible factor 1. J Natl Cancer Inst. 2003;95(7):516-25.https://doi.org/10.1093/jnci/95.7.516

Legend

Figure 1. Female db/db mice exhibit left ventricular hypertrophy, diastolic impairment, and myocardial fibrosis at 22 weeks. (A) Representative longitudinal Masson's trichrome staining of myocardial sections from female db/m and db/db mice at the indicated ages. (B) Representative gross heart images and quantification of HW/BW and LVW/BW in 22-week-old female db/m and db/db mice.
(C) Representative M-mode echocardiographic images and quantification of left ventricular mass, left ventricular anterior wall thickness at end-systole and end-diastole (LVAW,s and LVAW,d), and left ventricular posterior wall thickness at end-systole and end-diastole (LVPW,s and LVPW,d) in 22-week-old female db/m and db/db mice.
(D) Assessment of diastolic function by echocardiography, presented as E/A ratio. (E) Representative Masson's trichrome staining images and quantification of myocardial fibrosis in 22-week-old female db/m and db/db mice. (F) Western blot analysis and densitometric quantification of MYH7, COL1A1, and NPPA protein expression in myocardial tissue. α-Tubulin was used as a loading control. (G) Representative wheat germ agglutinin (WGA)

staining images and quantification of cardiomyocyte cross-sectional area in 22-week-old female db/m and db/db mice.
Data are presented as mean ± SEM. Each dot represents one mouse. Statistical significance was determined as indicated in the figure.

Figure 2. Female db/db mice exhibit greater cardiac hypertrophy, myocardial fibrosis, and diastolic impairment than male db/db mice at 22 weeks.
(A) Representative gross heart images and quantification of HW/BW and LVW/BW in 22-week-old female and male db/db mice. (B) Representative M-mode echocardiographic images and quantification of left ventricular structural parameters, including left ventricular posterior wall thickness at end-diastole (LVPWd) and end-systole (LVPWs), and left ventricular mass (LV mass). (C) Mitral valve E/A ratio assessed by echocardiography in 22-week-old female and male db/db mice, reflecting impaired diastolic relaxation in female mice. (D) Representative Masson's trichrome staining images (scale bar, 50 μm) and quantification of myocardial fibrotic area percentage in female and male db/db mice. (E) Representative HE staining and WGA staining images (scale bar, 50 μm) with quantification of cardiomyocyte cross-sectional area in female and male db/db mice. (F) Quantitative RT-PCR analysis of Myh7, Col1a1, and Nppa mRNA expression in myocardial tissue from female and male db/db mice. (G) Representative western blot images and densitometric quantification of MYH7, COL1A1, and NPPA protein expression in myocardial tissue. α-TUBULIN was used as the loading control.
Data are presented as mean ± SEM. Each dot represents one mouse. Statistical comparisons were performed as indicated.

Figure 3. Estrogen deficiency promotes cardiac remodeling in female db/db mice, and GPER activation is cardioprotective.
(A) Representative gross images of uterine horns from 22-week-old female db/m and db/db mice, demonstrating uterine atrophy in db/db animals. (B) Representative histological

cross-sections of ovaries from female db/m and db/db mice, showing ovarian atrophy in db/db animals. (C) Longitudinal serum estradiol (E2) levels measured at 8, 16, 20, and 22 weeks in female db/m and db/db mice. Data are presented as mean ± SEM.
(D) Representative gross cardiac images and quantification of HW/BW in female db/db mice treated with vehicle (Ctrl), E2, E2+G15, or G1. (E) Representative Masson's trichrome staining images and quantification of myocardial fibrotic area percentage across treatment groups. (F) Representative echocardiographic Doppler waveforms and quantification of the mitral valve E/A ratio across treatment groups, reflecting diastolic function.
(G) Representative echocardiographic images, including B-mode images in the upper row and M-mode images in the lower row, with quantification of LVAW,s, LVAW,d, LVPW,s, and LVPW,d across the treatment groups.(H) Representative western blot images and densitometric quantification of MYH7, COL1A1, and NPPA protein expression across treatment groups. α-TUBULIN was used as the loading control.
Data are presented as mean ± SEM. Each dot represents one mouse. Statistical comparisons were performed as indicated.

Figure 4. Estrogen and GPER activation attenuate high-glucose-induced hypertrophy and apoptosis in H9c2 cardiomyoblasts.
(A) Representative western blot images and densitometric quantification of MYH7 (220 kDa), COL1A1 (200 kDa), and NPPA (27 kDa) protein expression in H9c2 cells treated with normal glucose (NG, 5.5 mM) or high glucose (HG, 33 mM) for 48 hours. α-TUBULIN (55 kDa) served as the loading control. (B) Representative western blot images and densitometric quantification of BAX (21 kDa) and BCL2 (21 kDa) protein expression in HG-treated H9c2 cells following treatment with vehicle (Ctrl, DMSO), 17β-estradiol (E2, 100 nM), E2 combined with the GPER antagonist G15 (E2+G15, 100 nM E2 + 10 μM G15), or the selective GPER agonist G1 (10 μM). α-TUBULIN (55 kDa) served as the loading control. (C) Representative brightfield microscopy images of H9c2 cell morphology across treatment groups. (Scale bar, 200 μm) (D) Representative TUNEL

staining images and quantification of apoptotic cell percentage across treatment groups. (Scale bar, 50 μm.)(E) Representative western blot images and densitometric quantification of MYH7, COL1A1, and NPPA protein expression in HG-treated H9c2 cells across the four treatment groups described in (B). α-TUBULIN (55 kDa) served as the loading control.

Data are presented as mean ± SEM (n = 3–6 per group). Statistical comparisons were performed by one-way ANOVA with post hoc testing; p-values are shown on graphs.

Figure 5. Transcriptomic profiling of cardiac tissue identifies HIF-1 signaling as the predominant pathway regulated by GPER activation in female db/db mice.

Heatmap of differentially expressed genes in cardiac tissue from female db/db mice treated with G1 or vehicle (Ctrl). Each row represents one biological replicate, and each column represents one gene. Rows are annotated according to treatment group.Red indicates relatively high expression; blue indicates relatively low expression. (B) Volcano plot depicting differentially expressed genes between vehicle-treated (Ctrl) and G1-treated female db/db myocardium. Red dots: significantly upregulated genes in G1 group (n = 59); blue dots: significantly downregulated genes (n = 73); grey dots: non-significant. Dashed lines denote thresholds of $|\log_2 FC| > 1$ and adjusted $p < 0.05$. (C) KEGG pathway enrichment analysis of differentially expressed genes identified in G1-treated versus control cardiac tissue. Red bars represent the number of genes associated with each pathway, whereas the cyan line and square markers represent $-\log_{10}$ (adjusted P value). The HIF-1 signaling pathway (highlighted) showed the highest statistical significance.

Figure 6. GPER activation suppresses the HIF-1α/ANGPT2/VEGFA axis and promotes HIF-1α ubiquitination in diabetic cardiac tissue.

(A) Quantitative RT-PCR analysis of Angpt2, Vegfa, and Hif-1α mRNA expression in cardiac tissue from female db/db mice treated with vehicle (Ctrl) or G1. Expression levels were normalized to Gapdh and presented as relative values. (B) Representative western

blot images and densitometric quantification of ANGPT2 (65 kDa), VEGFA (25 kDa), and HIF-1α (125 kDa) protein expression in cardiac tissue from Ctrl and G1-treated female db/db mice. α-TUBULIN (55 kDa) was used as the loading control.

(C) Co-immunoprecipitation analysis of HIF-1α ubiquitination in cardiac tissue. Input samples from Ctrl and G1-treated mice, an IgG immunoprecipitation control, and HIF-1α-immunoprecipitated fractions from Ctrl and G1-treated mice are shown. The upper panel was immunoblotted for ubiquitin, and the lower panel was immunoblotted for HIF-1α. Increased ubiquitination of HIF-1α was observed in G1-treated cardiac tissue.

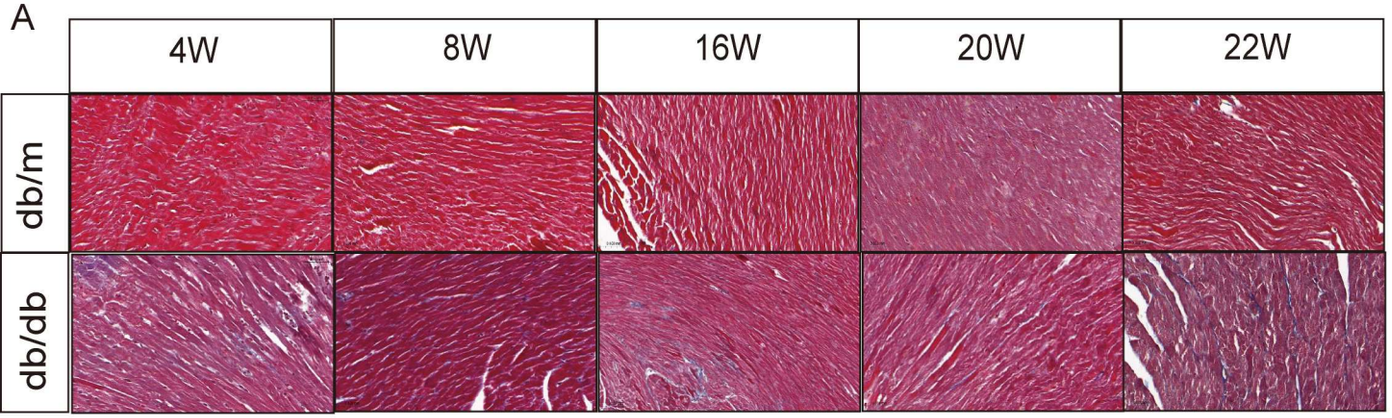
Data are presented as mean ± SEM (n = 3–6 per group). Statistical significance was determined by unpaired Student's t-test; p-values are shown on graphs.

Figure 7. Effects of YC-1 co-treatment on G1-mediated regulation of HIF-1α-related signaling and cardiomyocyte injury under high-glucose conditions.

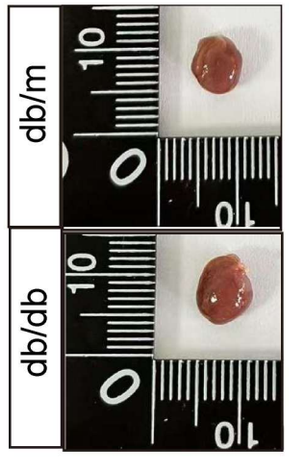
(A) Quantitative RT-PCR analysis of Angpt2, Vegfa, and Hif-1α mRNA expression in H9c2 cells subjected to HG treatment with vehicle (HG), G1 (10 μM), or G1+YC-1. Data are normalized to HG group. (B) Representative western blot images and densitometric quantification of ANGPT2 (65 kDa), VEGFA (25 kDa), and HIF-1α (125 kDa) protein expression. α-TUBULIN (55kDa) served as loading control. (C) Representative western blot images and densitometric quantification of hypertrophy/fibrosis markers MYH7 (220 kDa), COL1A1 (200 kDa), and NPPA (27 kDa) across treatment groups.α-TUBULIN (55 kDa) served as loading control. (D) Representative brightfield microscopy images illustrating H9c2 cell morphology in HG, G1, and G1+YC-1 groups. Scale bar, 200 μm. (E) Representative TUNEL staining images and quantification of the percentage of apoptotic cells across treatment groups. Scale bar, 50 μm.

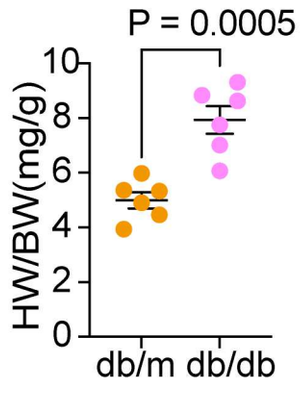
Data are presented as mean ± SEM. The number of biological replicates is indicated by the individual data points. Statistical significance was determined as indicated; p-values shown on graphs.

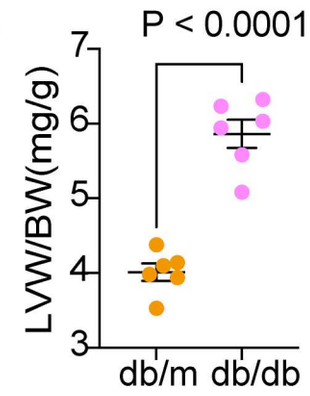
A


4W
8W
16W
20W
22W
db/m
db/db

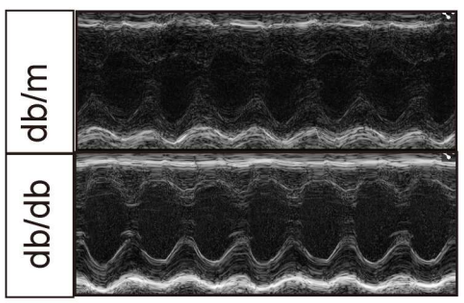
B

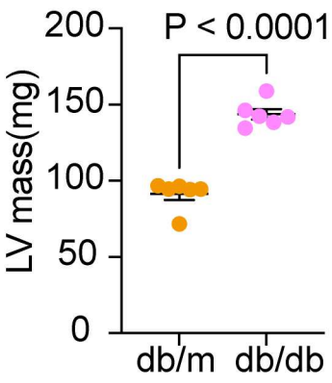

db/m
db/db

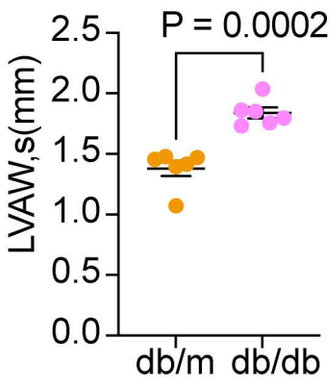

P = 0.0005
HW/BW(mg/g)
db/m db/db

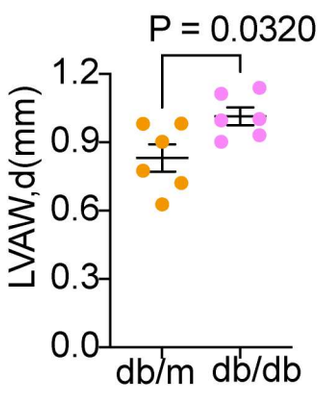

P < 0.0001
LVW/BW(mg/g)
db/m db/db

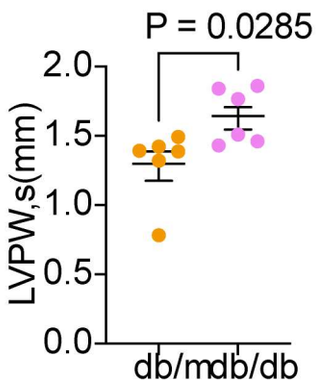
C

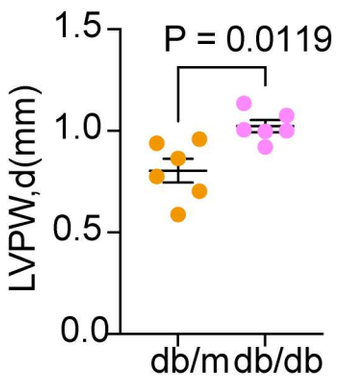

db/m
db/db


P < 0.0001
LV mass(mg)
db/m db/db

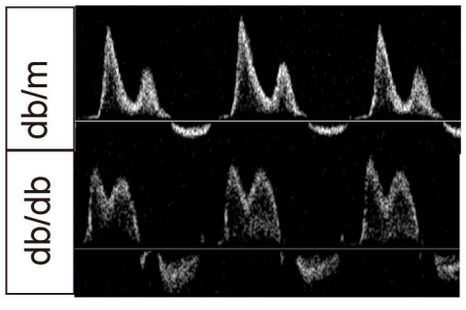

P = 0.0002
LVAW,s(mm)
db/m db/db

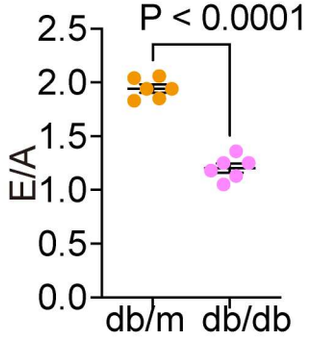

P = 0.0320
LVAW,d(mm)
db/m db/db


P = 0.0285
LVPW,s(mm)
db/m db/db

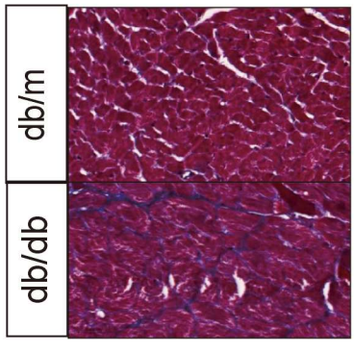

P = 0.0119
LVPW,d(mm)
db/m db/db

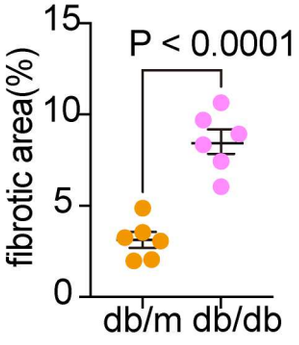
D


db/m
db/db

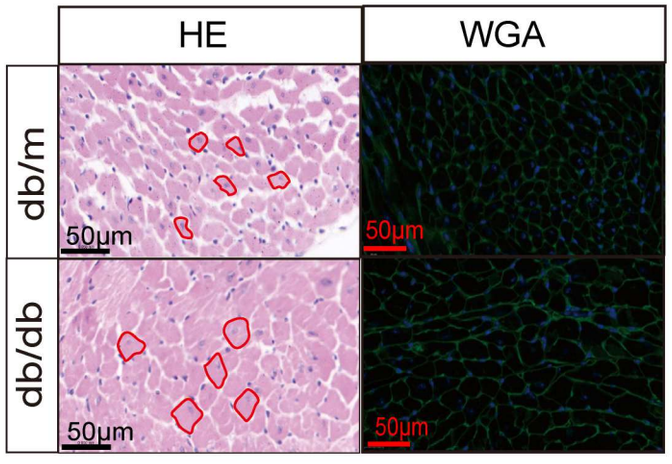

P < 0.0001
E/A
db/m db/db

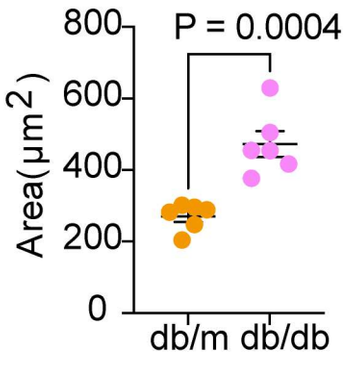
E


db/m
db/db

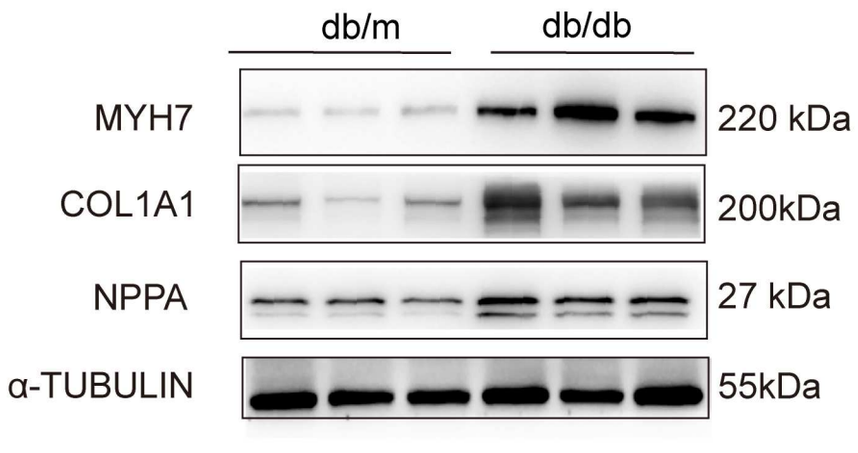

P < 0.0001
fibrotic area(%)
db/m db/db

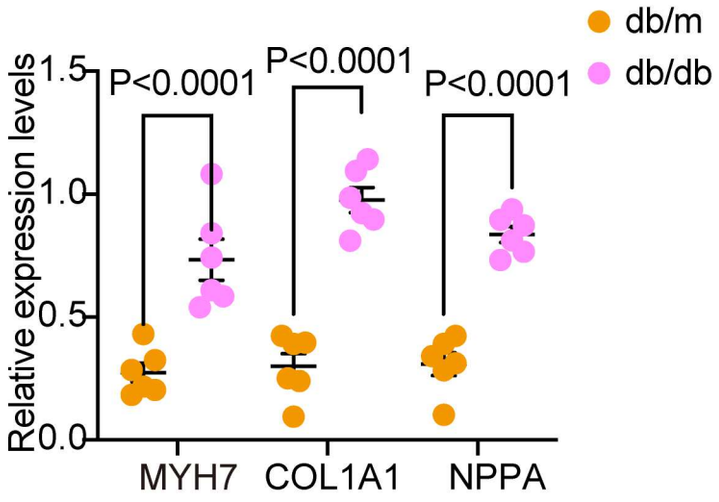
G

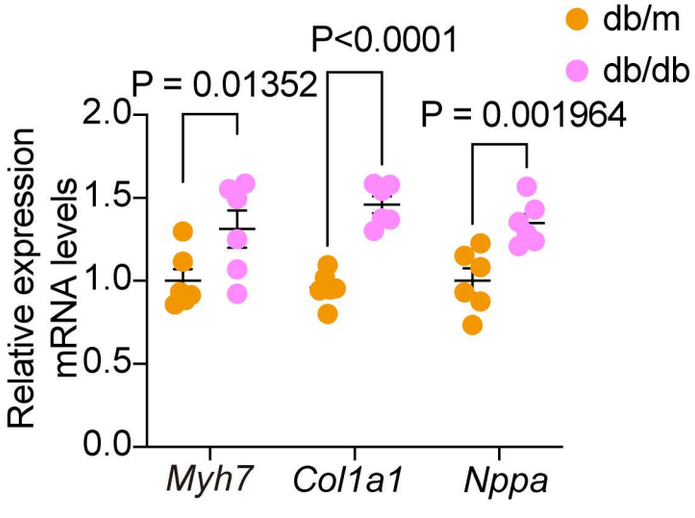

HE
WGA
db/m
db/db
50μm

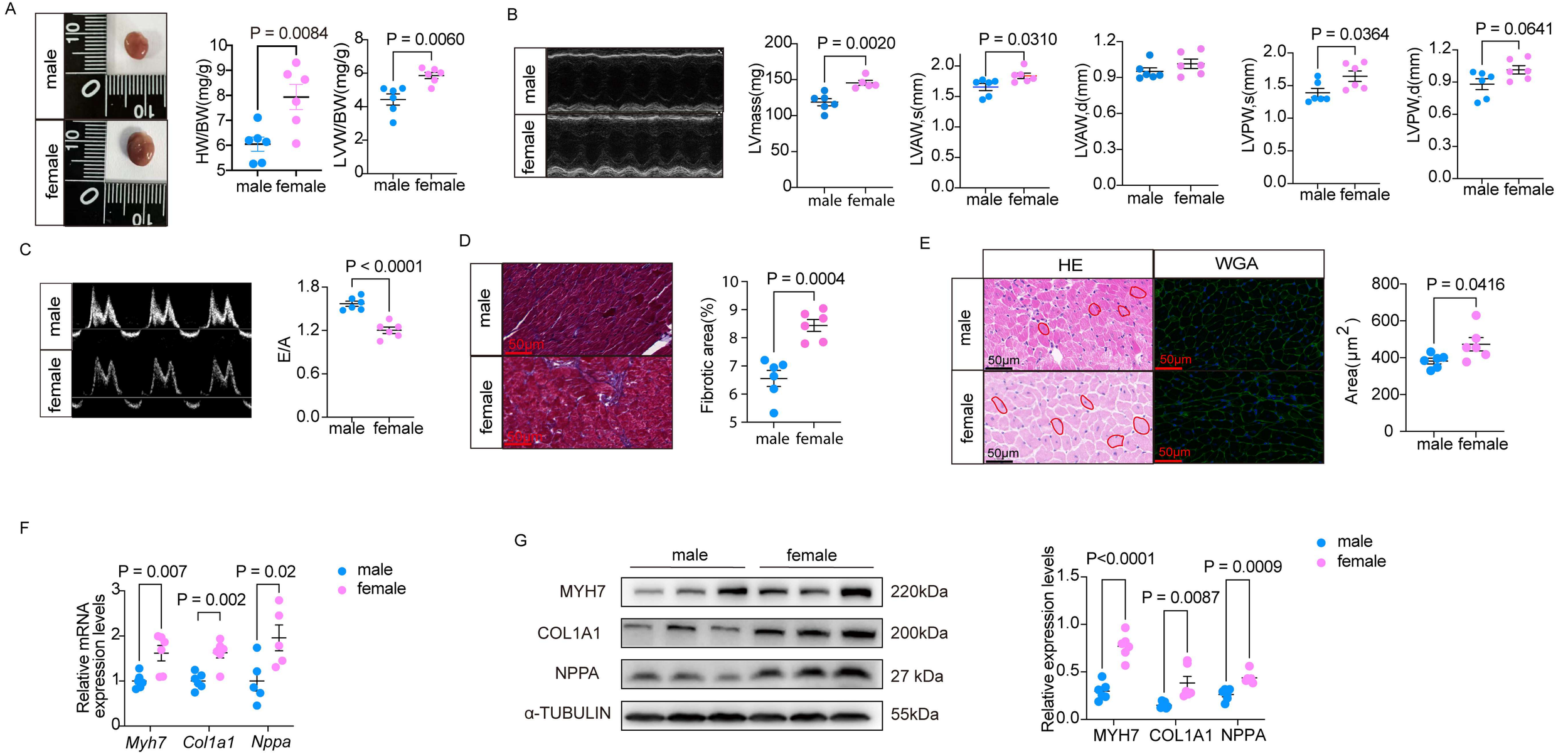

P = 0.0004
Area(μm2)
db/m db/db

F

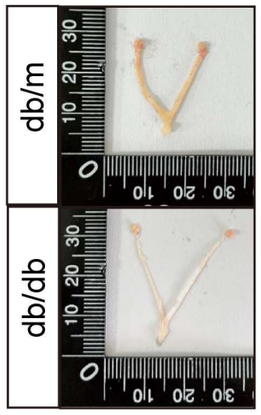

db/m
db/db
MYH7
COL1A1
NPPA
α-TUBULIN
220 kDa
200kDa
27 kDa
55kDa


db/m
db/db
P<0.0001
P<0.0001
P<0.0001
Relative expression levels
MYH7 COL1A1 NPPA

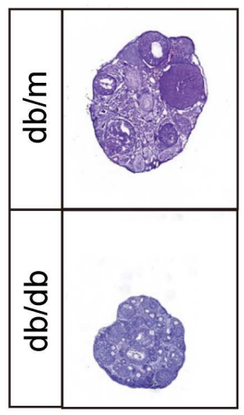

db/m
db/db
P<0.0001
P = 0.01352
P = 0.001964
Relative expression mRNA levels
Myh7 Col1a1 Nppa


A
male
female
HW/BW(mg/g)
P = 0.0084
male female
LVW/BW(mg/g)
P = 0.0060
male female
B
male
female
LVmass(mg)
P = 0.0020
male female
LVAW,s(mm)
P = 0.0310
male female
LVAW,d(mm)
male female
LVPW,s(mm)
P = 0.0364
male female
LVPW,d(mm)
P = 0.0641
male female
C
male
female
E/A
P < 0.0001
male female
D
male
female
50μm
Fibrotic area(%)
P = 0.0004
male female
E
HE
WGA
male
female
50μm
Area(μm2)
P = 0.0416
male female
F
Relative mRNA expression levels
P = 0.007
P = 0.002
P = 0.02
male
female
Myh7
Col1a1
Nppa
G
male
female
MYH7
COL1A1
NPPA
α-TUBULIN
220kDa
200kDa
27 kDa
55kDa
Relative expression levels
P<0.0001
P = 0.0087
P = 0.0009
male
female
MYH7
COL1A1
NPPA

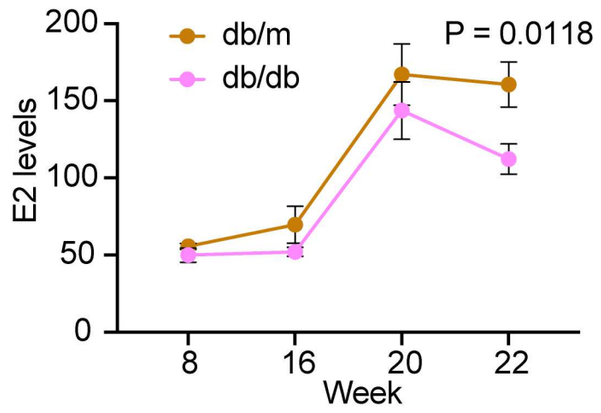
A


db/m
db/db

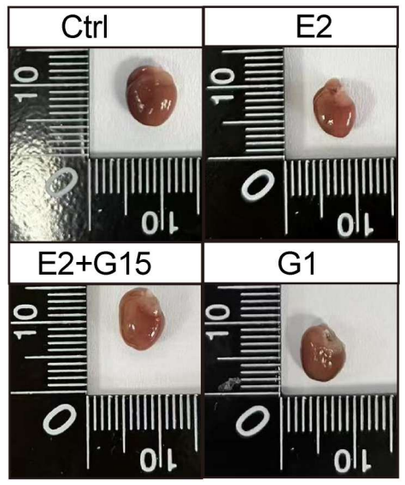
B

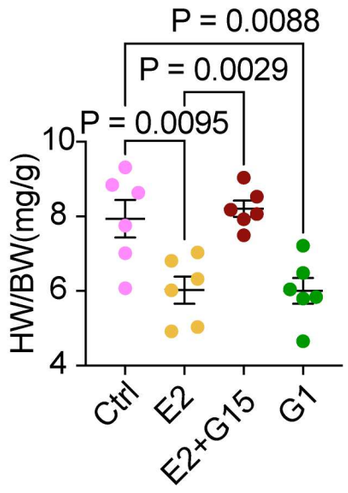

db/m
db/db

C

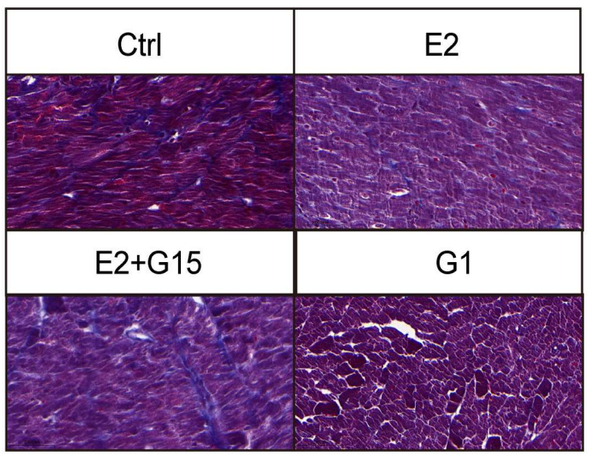

db/m
db/db
P = 0.0118
E2 levels
200
150
100
50
0
8
16
20
22
Week

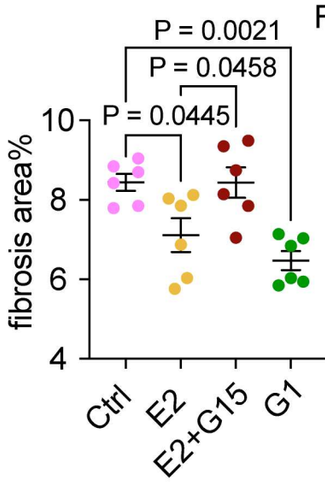
D


Ctrl
E2
E2+G15
G1

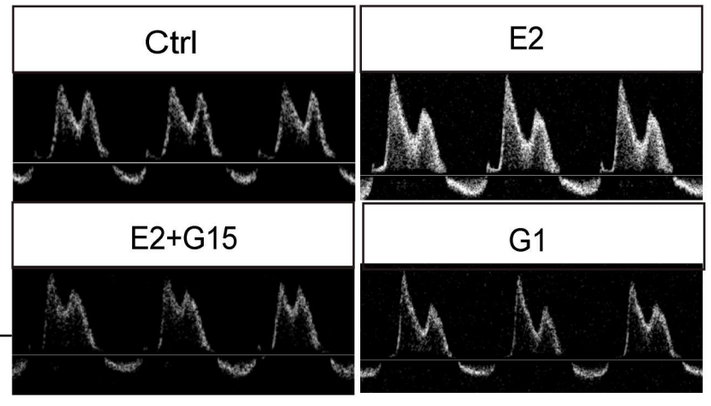

P = 0.0088
P = 0.0029
P = 0.0095
HW/BW(mg/g)
10
8
6
4
Ctrl
E2
E2+G15
G1

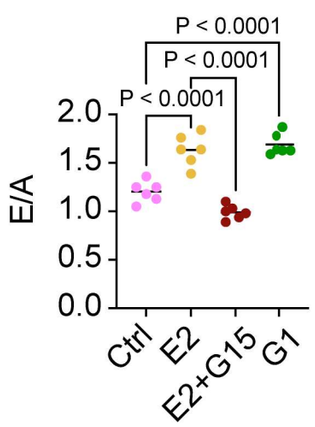
E

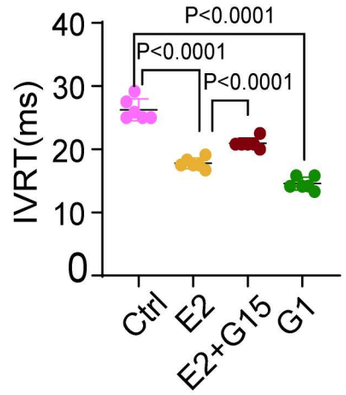

Ctrl
E2
E2+G15
G1


P = 0.0021
P = 0.0458
P = 0.0445
fibrosis area%
10
8
6
4
Ctrl
E2
E2+G15
G1

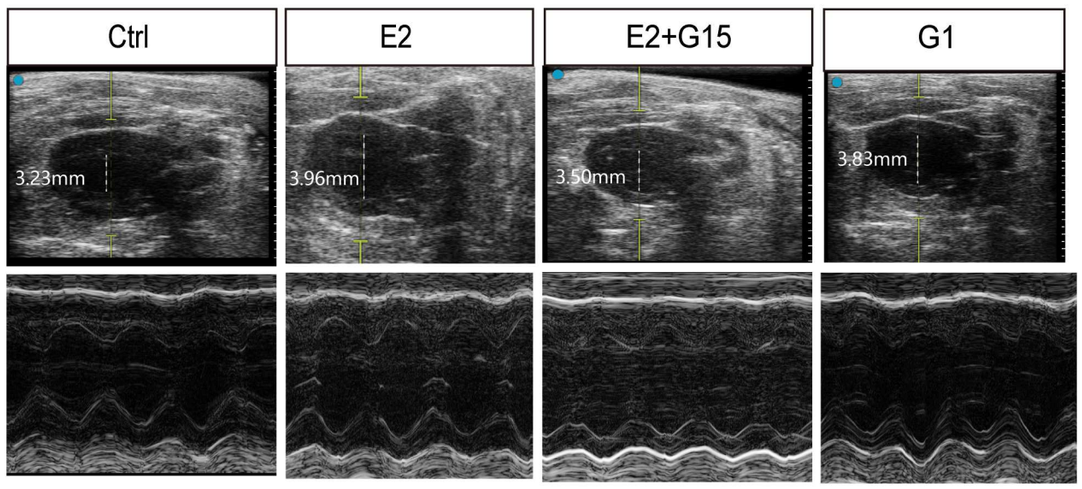
F

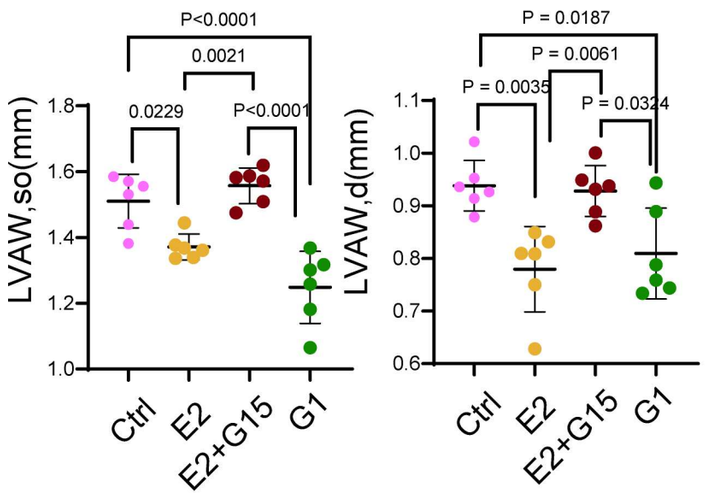

Ctrl
E2
E2+G15
G1


P < 0.0001
P < 0.0001
P < 0.0001
E/A
2.0
1.5
1.0
0.5
0.0
Ctrl
E2
E2+G15
G1

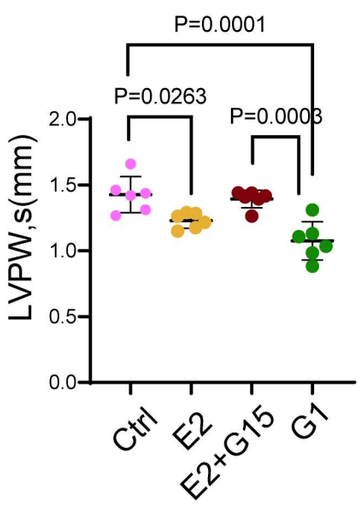

P<0.0001
P<0.0001
P<0.0001
IVRT(ms)
40
30
20
10
0
Ctrl
E2
E2+G15
G1

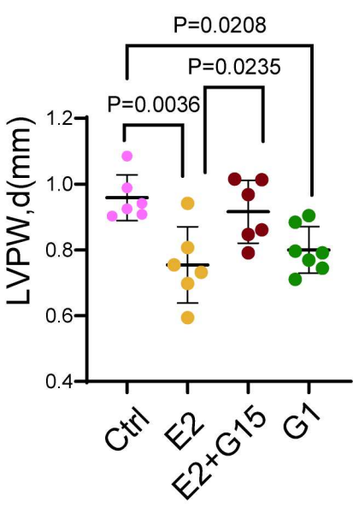
G


Ctrl
E2
E2+G15
G1
3.23mm
3.96mm
3.50mm
3.83mm

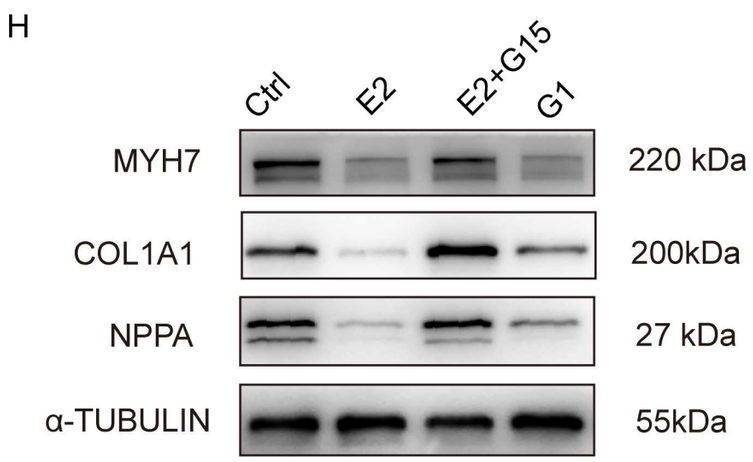

P<0.0001
0.0021
0.0229
P<0.0001
LVAW,so(mm)
1.8
1.6
1.4
1.2
1.0
Ctrl
E2
E2+G15
G1

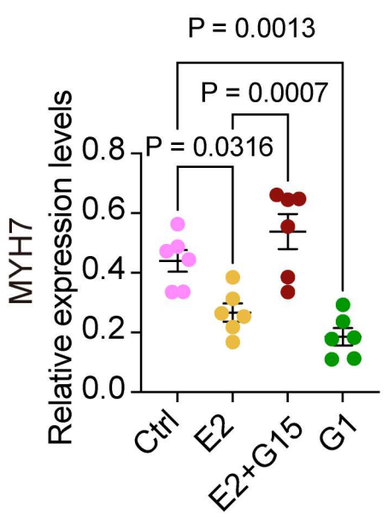
P = 0.0187
P = 0.0061
P = 0.0035
P = 0.0324
LVAW,d(mm)
1.1
1.0
0.9
0.8
0.7
0.6
Ctrl
E2
E2+G15
G1

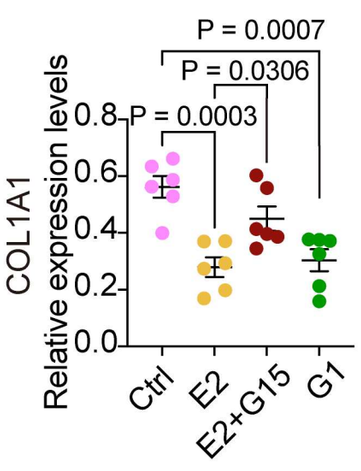

P=0.0001
P=0.0263
P=0.0003
LVPW,s(mm)
2.0
1.5
1.0
0.5
0.0
Ctrl
E2
E2+G15
G1

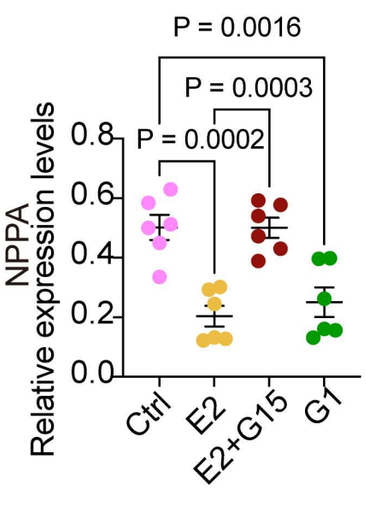

P=0.0208
P=0.0235
P=0.0036
LVPW,d(mm)
1.2
1.0
0.8
0.6
0.4
Ctrl
E2
E2+G15
G1

H

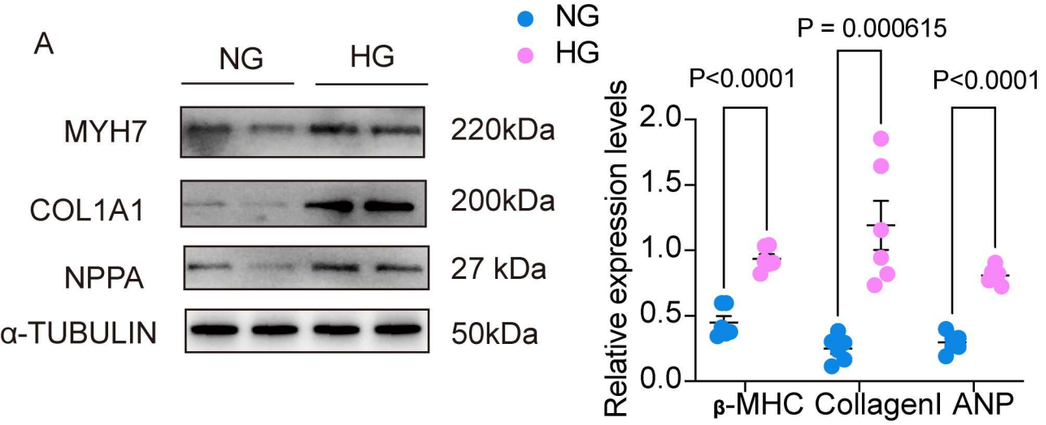

Ctrl
E2
E2+G15
G1
MYH7
220 kDa
COL1A1
200kDa
NPPA
27 kDa
α-TUBULIN
55kDa


P = 0.0013
P = 0.0007
P = 0.0316
MYH7
Relative expression levels
0.8
0.6
0.4
0.2
0.0
Ctrl
E2
E2+G15
G1

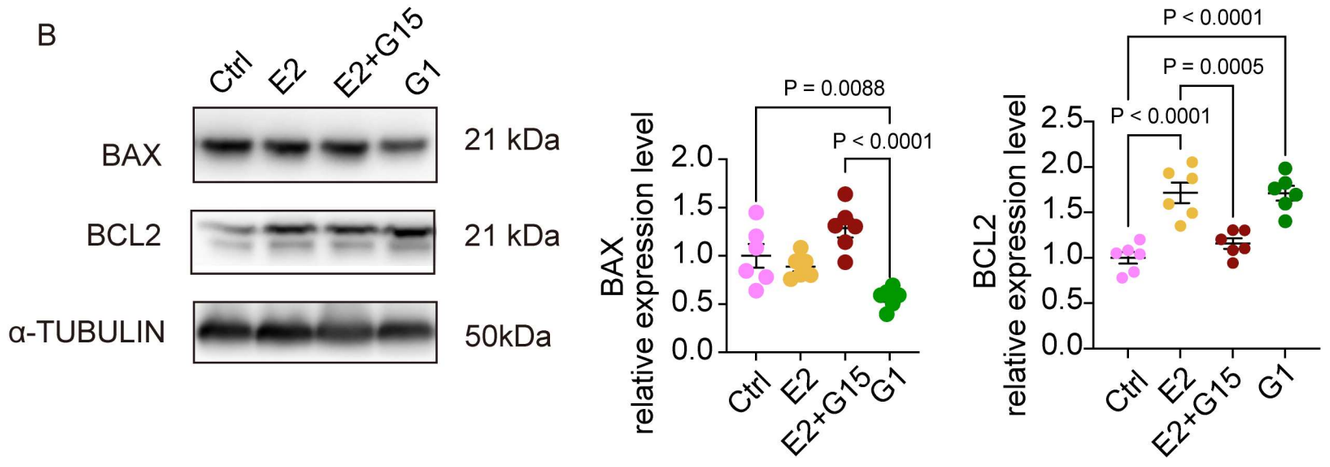

P = 0.0007
P = 0.0306
P = 0.0003
COL1A1
Relative expression levels
0.8
0.6
0.4
0.2
0.0
Ctrl
E2
E2+G15
G1


P = 0.0016
P = 0.0003
P = 0.0002
NPPA
Relative expression levels
0.8
0.6
0.4
0.2
0.0
Ctrl
E2
E2+G15
G1

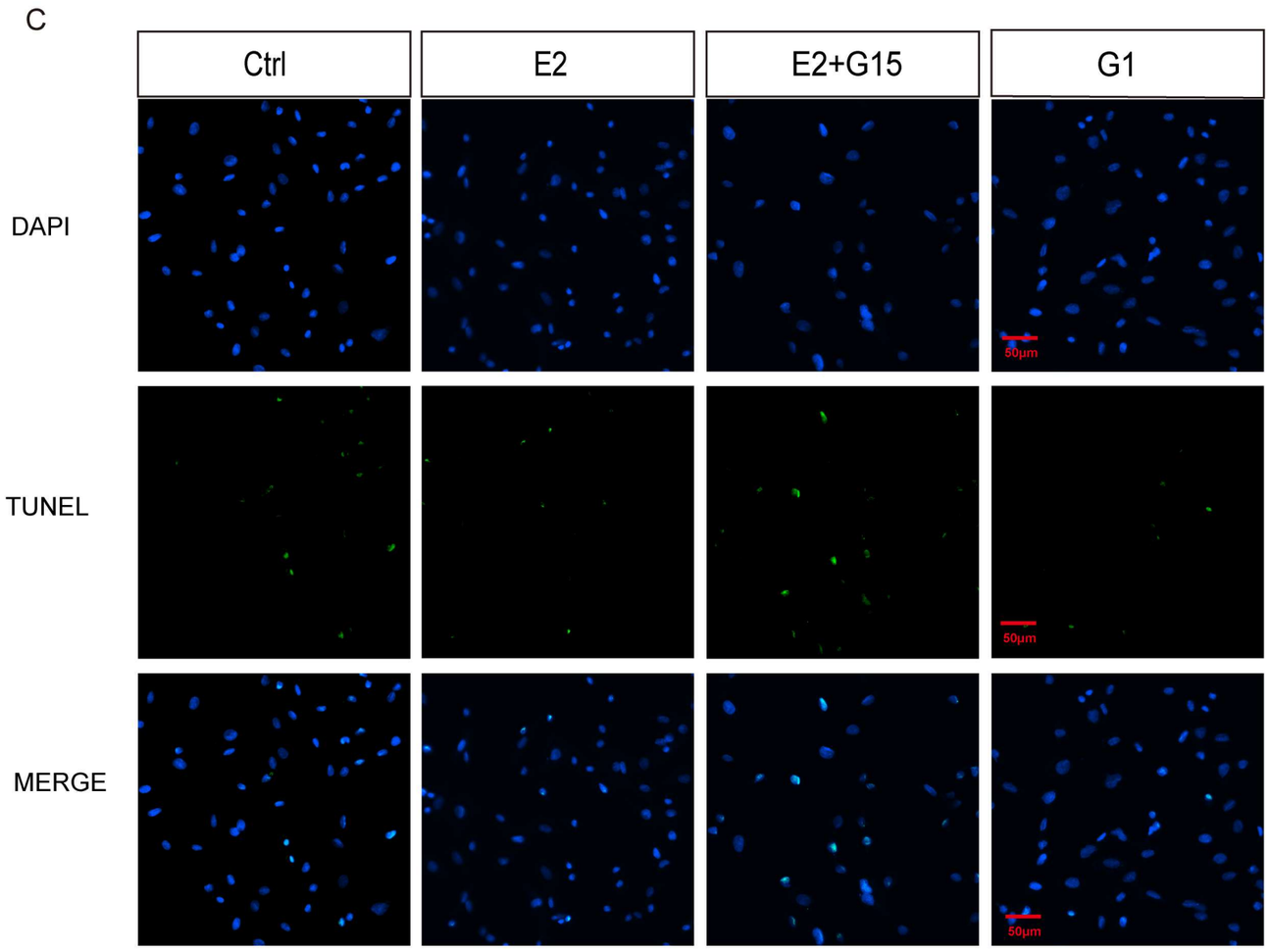
A

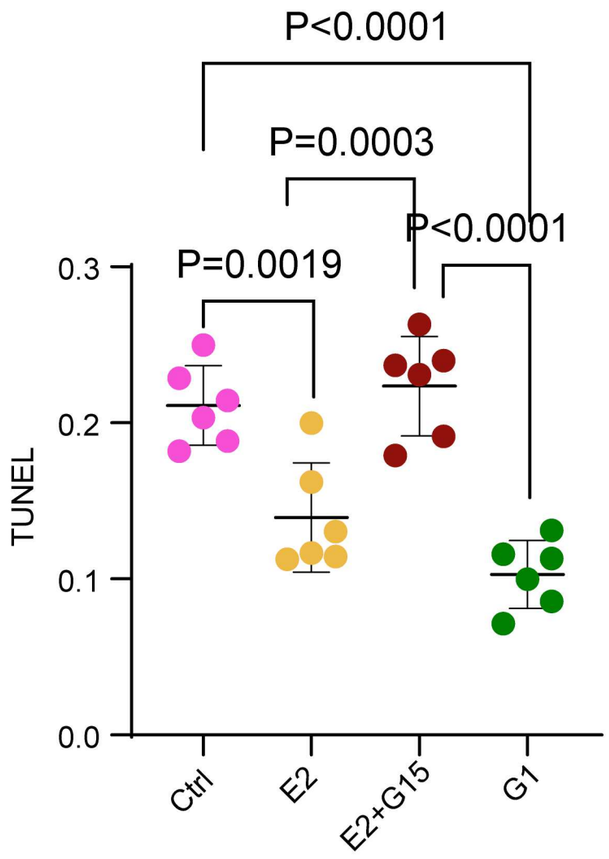

NG
HG
MYH7
COL1A1
NPPA
α-TUBULIN
220kDa
200kDa
27 kDa
50kDa
P = 0.000615
P<0.0001
P<0.0001
Relative expression levels
β-MHC CollagenI ANP

B

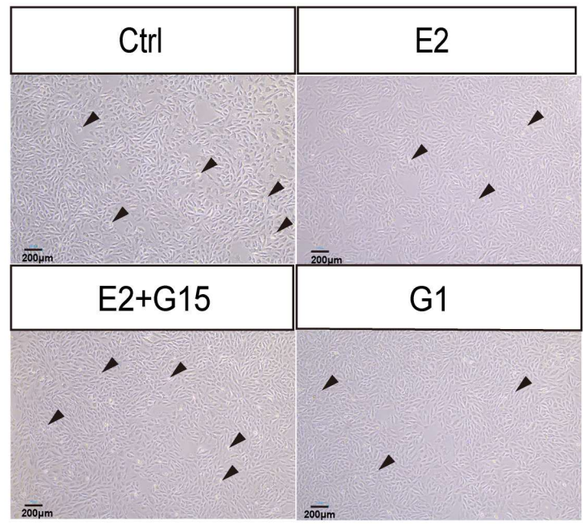

Ctrl
E2
E2+G15
G1
BAX
BCL2
α-TUBULIN
21 kDa
21 kDa
50kDa
P = 0.0088
P < 0.0001
BAX relative expression level
P < 0.0001
P = 0.0005
P < 0.0001
BCL2 relative expression level

C

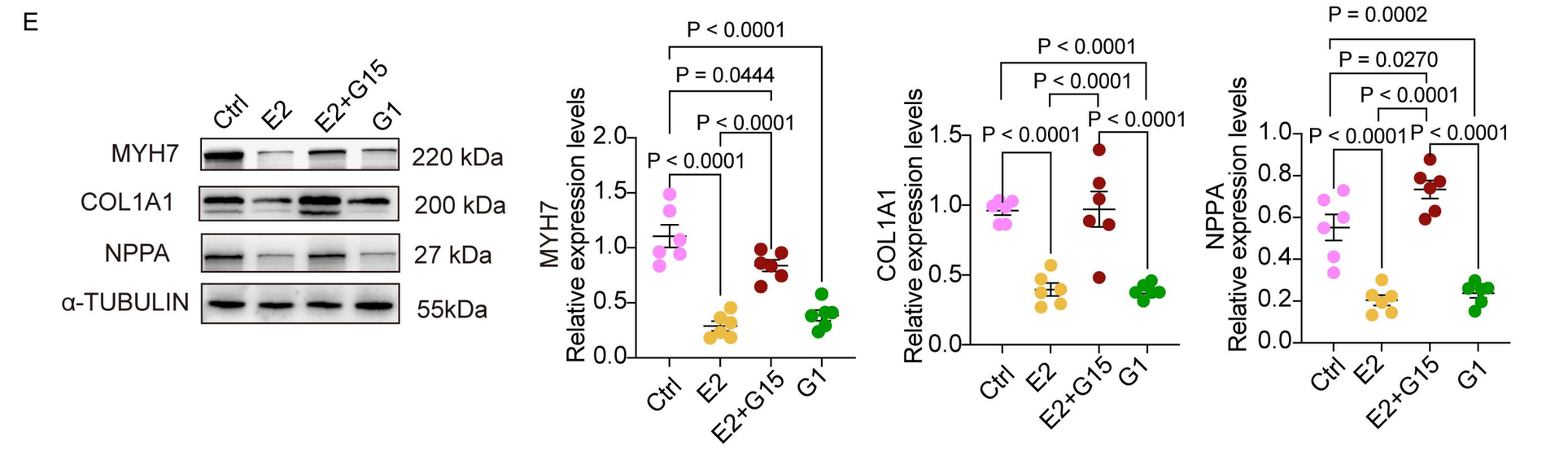

Ctrl
E2
E2+G15
G1
DAPI
TUNEL
MERGE
50μm


P<0.0001
P=0.0003
P<0.0001
P=0.0019
TUNEL
Ctrl
E2
E2+G15
G1

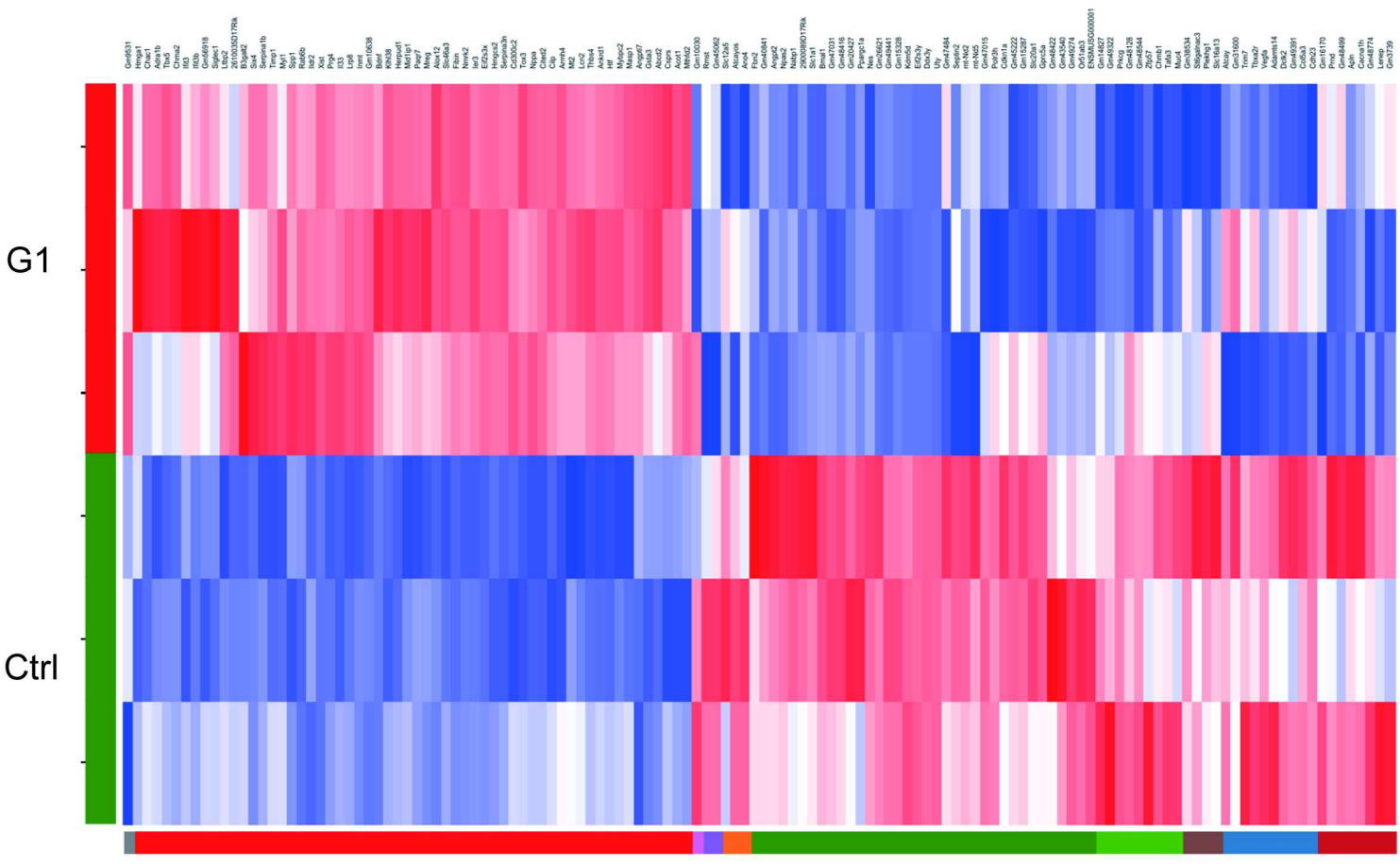
D


Ctrl
E2
E2+G15
G1
200μm

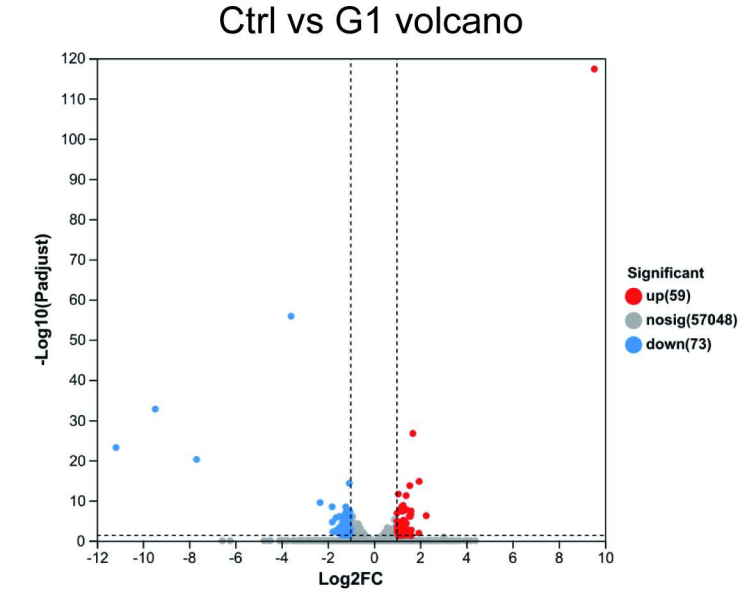
E


Ctrl
E2
E2+G15
G1
MYH7
COL1A1
NPPA
α-TUBULIN
220 kDa
200 kDa
27 kDa
55kDa
P < 0.0001
P = 0.0444
P < 0.0001
P < 0.0001
MYH7 Relative expression levels
P < 0.0001
P < 0.0001
P < 0.0001
P < 0.0001
COL1A1 Relative expression levels
P = 0.0002
P = 0.0270
P < 0.0001
P < 0.0001
P < 0.0001
NPPA Relative expression levels

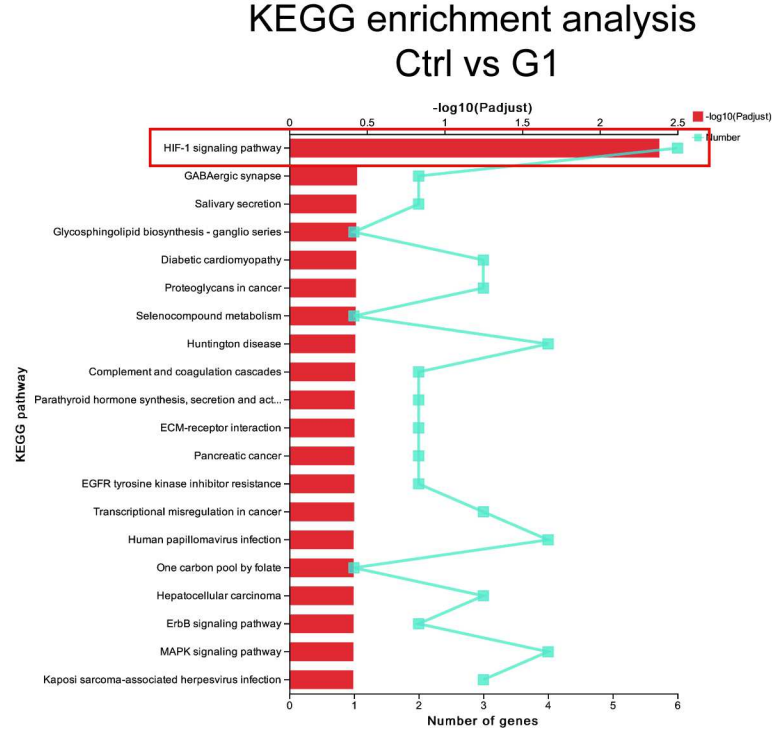
A

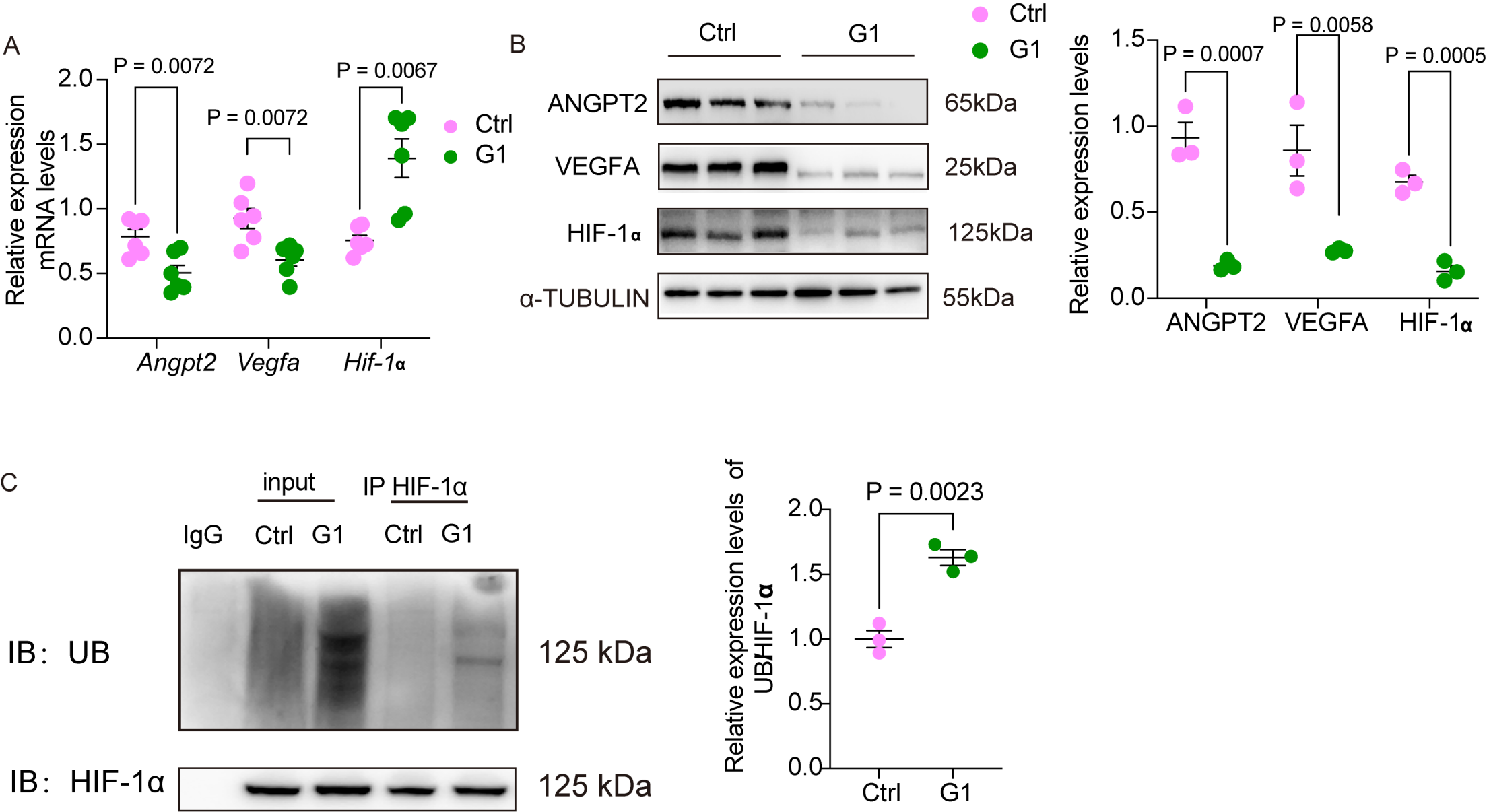

G1
Ctrl

B

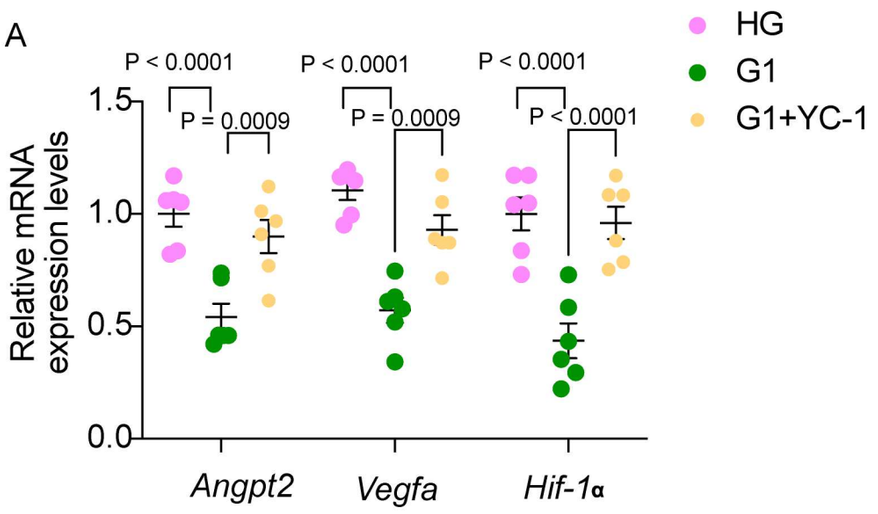

Ctrl vs G1 volcano
-Log10(Padjust)
Log2FC
Significant
up(59)
nosig(57048)
down(73)

C

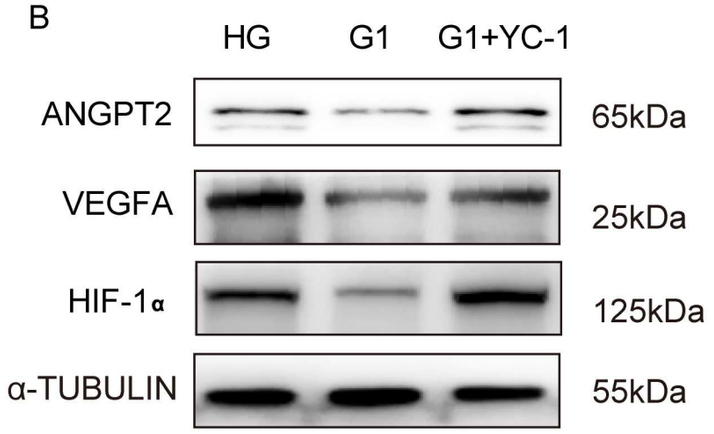

KEGG enrichment analysis
Ctrl vs G1
-log10(Padjust)
Number
HIF-1 signaling pathway
GABAergic synapse
Salivary secretion
Glycosphingolipid biosynthesis - ganglio series
Diabetic cardiomyopathy
Proteoglycans in cancer
Selenocompound metabolism
Huntington disease
Complement and coagulation cascades
Parathyroid hormone synthesis, secretion and act...
ECM-receptor interaction
Pancreatic cancer
EGFR tyrosine kinase inhibitor resistance
Transcriptional misregulation in cancer
Human papillomavirus infection
One carbon pool by folate
Hepatocellular carcinoma
ErbB signaling pathway
MAPK signaling pathway
Kaposi sarcoma-associated herpesvirus infection
KEGG pathway
Number of genes

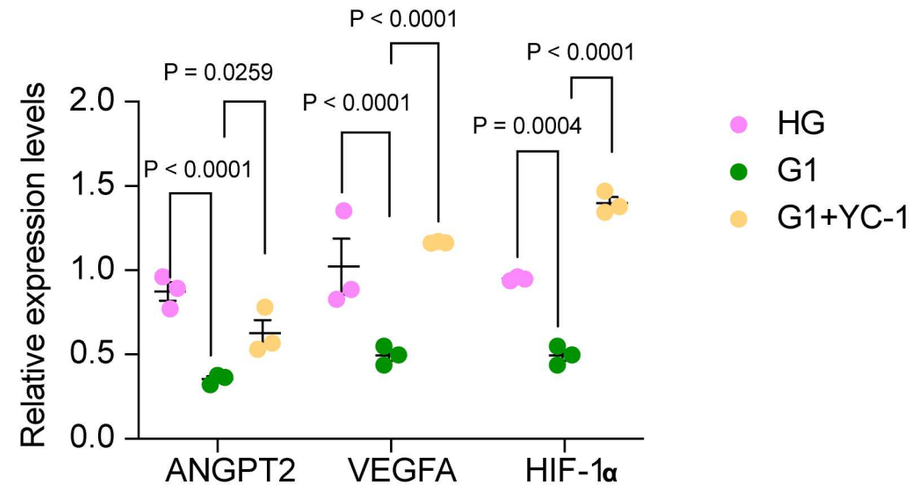

A
Relative expression mRNA levels
2.0
1.5
1.0
0.5
0.0
P = 0.0072
P = 0.0072
P = 0.0067
Ctrl
G1
Angpt2
Vegfa
Hif-1α
B
Ctrl
G1
ANGPT2
VEGFA
HIF-1α
α-TUBULIN
65kDa
25kDa
125kDa
55kDa
Ctrl
G1
Relative expression levels
1.5
1.0
0.5
0.0
P = 0.0007
P = 0.0058
P = 0.0005
ANGPT2
VEGFA
HIF-1α
C
input
IP HIF-1α
IgG
Ctrl
G1
Ctrl
G1
IB: UB
125 kDa
IB: HIF-1α
125 kDa
Relative expression levels of UBHIF-1α
2.0
1.5
1.0
0.5
0.0
P = 0.0023
Ctrl
G1

A

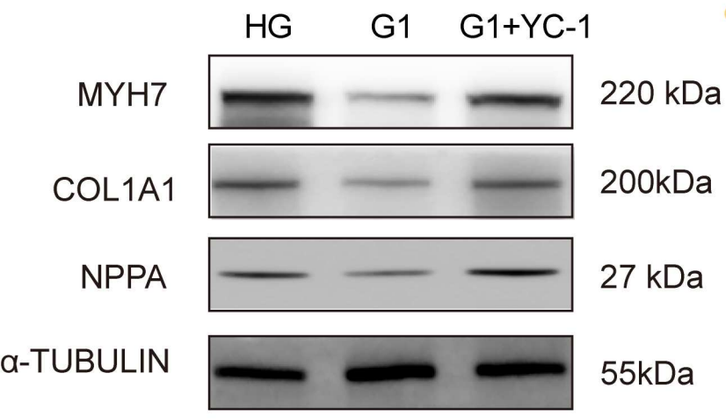

HG
G1
G1+YC-1
P < 0.0001
P < 0.0001
P < 0.0001
P = 0.0009
P = 0.0009
P < 0.0001
Relative mRNA expression levels
1.5
1.0
0.5
0.0
Angpt2
Vegfa
Hif-1α

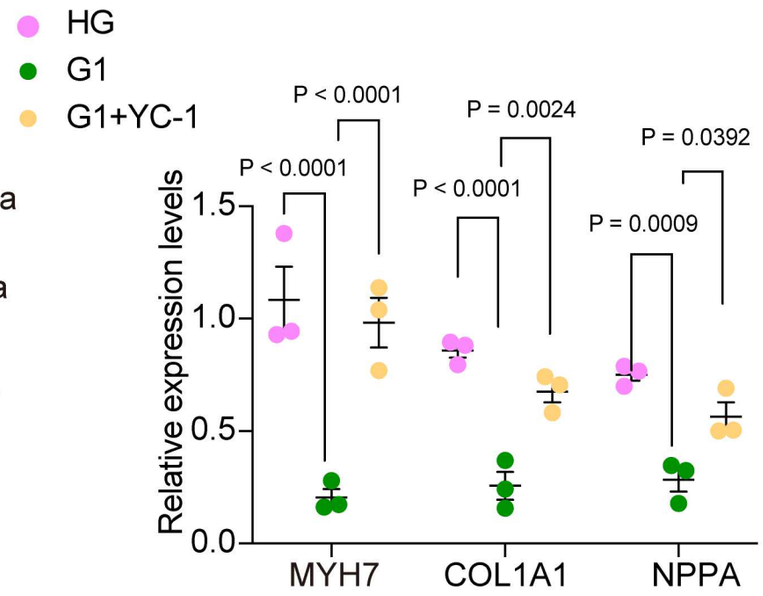
B


HG
G1
G1+YC-1
ANGPT2
VEGFA
HIF-1α
α-TUBULIN
65kDa
25kDa
125kDa
55kDa

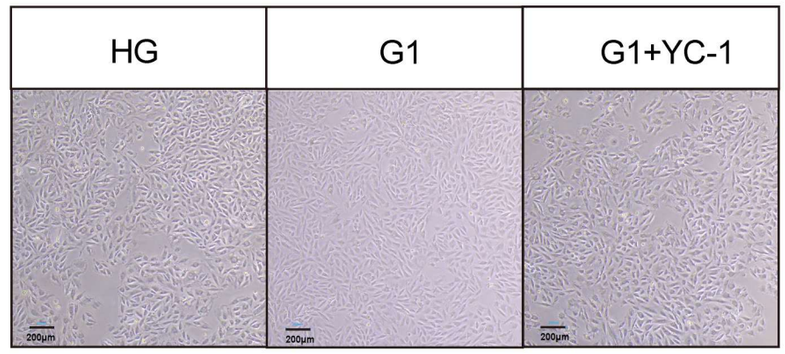

P < 0.0001
P = 0.0259
P < 0.0001
P < 0.0001
P = 0.0004
P < 0.0001
Relative expression levels
2.0
1.5
1.0
0.5
0.0
ANGPT2
VEGFA
HIF-1α
HG
G1
G1+YC-1

C

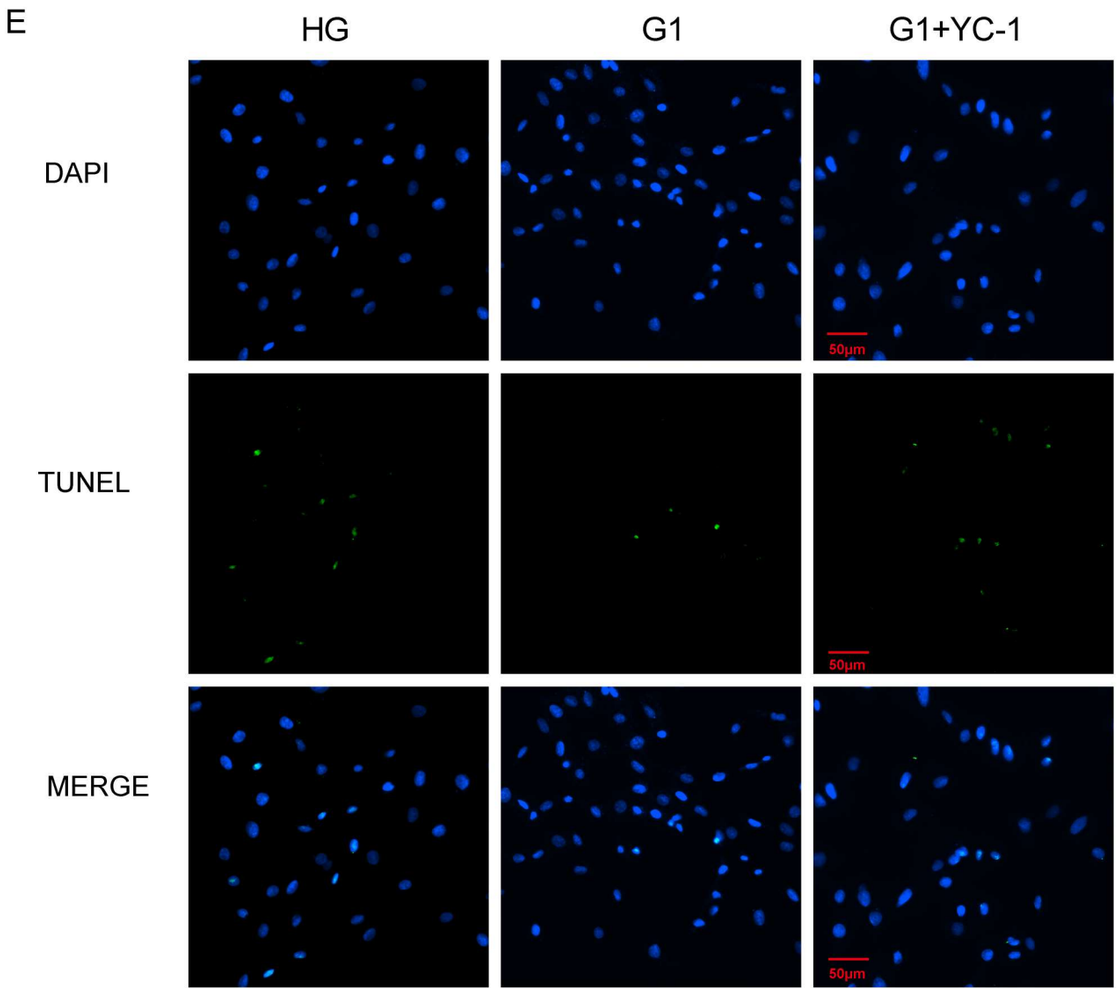

HG
G1
G1+YC-1
MYH7
COL1A1
NPPA
α-TUBULIN
220 kDa
200kDa
27 kDa
55kDa

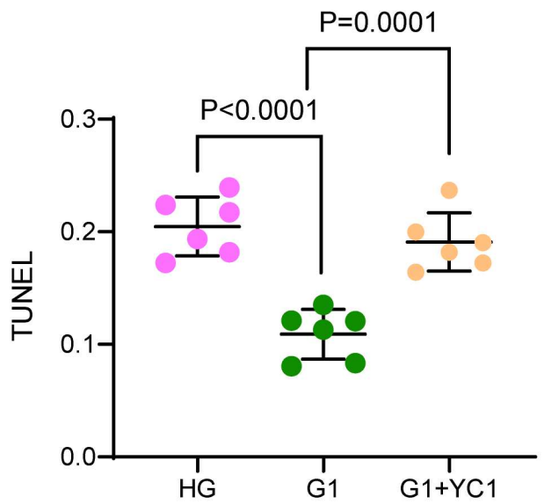

HG
G1
G1+YC-1
P < 0.0001
P < 0.0001
P < 0.0001
P = 0.0024
P = 0.0009
P = 0.0392
Relative expression levels
1.5
1.0
0.5
0.0
MYH7
COL1A1
NPPA

D


HG
G1
G1+YC-1
200μm
200μm
200μm

E


HG
G1
G1+YC-1
DAPI
TUNEL
MERGE
50μm
50μm
50μm


P=0.0001
P<0.0001
TUNEL
0.3
0.2
0.1
0.0
HG
G1
G1+YC1

Supplementary Files

This is a list of supplementary files associated with this preprint. Click to download.

- Table1011.docx